

Article

Seismic Performance Evaluation and Comparative Study of Reinforced Concrete Building on a Sloped Terrain with Regular Building by Considering the Effect of URM Infill Walls

Bush Rc ^{1,*} , Varsha Rani ^{2,*}, Mohamed F. Suleiman ³ , Bapugouda B. Biradar ^{1,4} , Rohit Vyas ¹ ,
Afaq Ahmad ⁵  and Anoop I. Shirkol ¹

¹ Department of Civil Engineering, Malaviya National Institute of Technology, Jaipur 302017, India; 2021rce9509@mnit.ac.in (B.B.B.); 2020rce9515@mnit.ac.in (R.V.); anoop.ce@mnit.ac.in (A.I.S.)

² Department of Civil Engineering, National Institute of Technology, Agartala 799046, India

³ College of Engineering, Civil Engineering Department, University of Tripoli, Tripoli 13932, Libya; m.suleiman@uot.edu.ly

⁴ School of Civil Engineering, KLE Technological University, Hubballi 580031, India

⁵ Department of Civil Engineering, College of Engineering, University of Memphis, Memphis, TN 38152, USA; aahmad4@memphis.edu

* Correspondence: 2021rce9516@mnit.ac.in (B.R.); varsharani085@gmail.com (V.R.)

Abstract: This paper focuses on the seismic vulnerabilities of multi-storey buildings in hilly regions like Sikkim and Uttarakhand, where rapid construction is driven by population growth and tourism. The study particularly evaluates step-back buildings on hilly slopes, comparing their vulnerability to standard buildings on flat terrain. Using non-linear analysis to assess structural aspects like displacement and storey drift ratio, the research examines the performance of these buildings in both uphill and downhill orientations against typical three-storey and six-storey structures, respectively. The findings indicate that step-back buildings, especially those without infill walls, are more susceptible to seismic damage. For instance, on the uphill side, a step-back building shows a mean drift ratio 15.11% greater in the X direction and 4.57% greater in the Y direction compared to a three-storey regular building (3SR). This vulnerability is exacerbated when infill walls are absent, with mean drift ratios in step-back buildings being 74.75% and 33% higher in the X and Y directions, respectively. Moreover, at a seismic acceleration of 0.36 g, the mean displacement of a step-back building is 83% greater in the X direction and 51% greater in the Y direction than those with infill walls (SBIN), underscoring the significant role of infill walls in enhancing earthquake resilience. The study also highlights that short columns in step-back buildings are particularly prone to severe damage, especially just above the uppermost foundation level. While infill walls offer substantial mitigation of damage at the Design Basis Earthquake (DBE) level, at the Maximum Considered Earthquake (MCE) level, step-back buildings still endure severe damage compared to regular buildings with infill walls. Consequently, the research establishes that step-back buildings demonstrate greater vulnerability at DBE levels without infill walls and are more susceptible to damage than flat terrain buildings at MCE levels, emphasizing the need for careful design and reinforcement strategies in earthquake-prone hilly areas.

Keywords: hilly slope; step-back building; infill wall; non-linear analysis



Citation: Rc, B.; Rani, V.; Suleiman, M.F.; Biradar, B.B.; Vyas, R.; Ahmad, A.; Shirkol, A.I. Seismic Performance Evaluation and Comparative Study of Reinforced Concrete Building on a Sloped Terrain with Regular Building by Considering the Effect of URM Infill Walls. *Buildings* **2024**, *14*, 33. <https://doi.org/10.3390/buildings14010033>

Academic Editors: Humberto Varum, Fernando F. S. Pinho and Wusheng Zhao

Received: 9 November 2023

Revised: 12 December 2023

Accepted: 19 December 2023

Published: 21 December 2023



Copyright: © 2023 by the authors. Licensee MDPI, Basel, Switzerland. This article is an open access article distributed under the terms and conditions of the Creative Commons Attribution (CC BY) license (<https://creativecommons.org/licenses/by/4.0/>).

1. Introduction

The population is always on the rise, especially in India. Scarcity in land availability forces people to stay on lesser available land. The situation is further complicated when the available land is uneven, such as in hilly regions. The design of buildings in hilly regions is a challenging task due to various reasons, such as uneven terrain, steep gradients, and the constant effects of natural hazards due to adverse climatic conditions. After the experience of heavy losses of life during past earthquakes like the Assam 2021 (*M_w* 6.4), Mizoram 2020

(*Mw* 5.5), Ambassa 2017 (*Mw* 5.7), Manipur 2016 (*Mw* 6.7), Nepal 2015 (*Mw* 7.8), Sikkim 2011 (*Mw* 6.8), Kashmir 2005 (*Mw* 7.6), and Uttarkashi 1991 (*Mw* 6.8) earthquakes, the construction of buildings on uneven terrain has improved a fair amount [1]. The types of building configurations generally preferred in a sloped terrain are step-back, set-back, and the combination of step-back, set-back, and split foundation. Based on the building alignment, buildings are categorised as step-back, set-back, and step-back set-back [2]. Foundations provided at various levels due to sloped terrain are called split foundations. Past studies in Uttarakhand reveal that most of the buildings constructed are of step-back and split foundation configuration [3,4]. Figure 1 shows a damaged RC building situated in the Nepal region [5]. The configurations of the models adopted in the present study are inspired by Figure 1. RC structures situated on different terrains perform differently. If the effect of uneven terrain is ignored, the structure may collapse during a minor earthquake [4]. A structure situated on an uneven terrain/hill region undergoes a torsional effect, which is due to the non-coincidence of the centre of mass and the centre of stiffness [4,6]. Failure in RC buildings on sloped terrain is usually due to the failure of the uppermost foundation. Because of the torsional effect, a proper study of the terrain profile and performance of the structure is important [6,7]. This research paper presents a novel investigation into how stepped buildings, particularly those on uneven or hilly terrains, respond to earthquakes. It focuses on an area not extensively covered in previous studies: the specific seismic responses of stepped structures. The study involves modelling an idealized six-storey step-back building, akin to one that previously failed, and compares its uphill side to a three-storey regular building and its downhill side to a six-storey regular building. This comparison yields fresh insights into the structural behaviour and integrity of stepped buildings under earthquake conditions. SAP2000 [8] was used for non-linear static and dynamic analyses of structures on uneven terrain or hilly slopes, aimed at evaluating their performance under varying conditions. An idealized six-storey step-back building was modelled (similar to the failed building shown in Figure 1). The uphill side of the model was compared to a three-storey regular building. Similarly, the downhill-side model was compared to a six-storey regular building.



Figure 1. Damaged RC building resting on sloped terrain affected by the 2015 Nepal earthquake [5].

2. Past Studies

Birajdal et al. [9] conducted a comparative study focusing on three building designs: set-back, step-back, and set-back step-back. Their findings revealed that buildings with a short-column and set-back design are especially prone to high torsional moments, making them more susceptible to damage. The study highlighted that on sloped terrains, the columns' varying heights lead to an uneven distribution of stiffness. This results in short columns, which are stiffer, bearing the brunt of the maximum storey shear. Singh et al. [6] also explored this topic, concluding that short columns, due to their high stiffness, are effective in resisting the maximum storey shear [4].

An extensive investigation into the building failures during the Sikkim earthquake corroborated similar findings, with Gosh et al. [10] examining how soil–structure interaction affects buildings on sloped terrains and focusing on variations in slope angles. Their research concluded that a building's vulnerability escalates with an increase in the slope angle, primarily due to the irregular distribution of column stiffness, which causes more movement on the taller side than the shorter side. In a related study, Halder et al. [1] explored the design quality of buildings on slopes and the impact of unevenly distributed infill walls, while Liu et al. [11] focused on a building with a step-back set-back configuration, developing a model that incorporates soil–structure interaction for simulating earthquake excitation. Using the elastoplastic method to determine the structural responses, they found that buildings with a step-back set-back design experienced less damage due to the distribution of plastic hinges compared to other configurations, leading the authors to underscore the importance of including soil–structure interaction in designs to mitigate damage or failure in hilly regions.

In an effort to gauge the effectiveness of infill walls, a study compared structures with infill walls to bare-frame structures, concluding that the addition of infill walls significantly enhances a structure's strength. Complementing this research, Kumar [12] delved into various types of buildings in sloped regions, pinpointing key issues for these building types. His conclusions emphasized that parameters such as topography, vegetation, soil structure, and slope angle are crucial and should be incorporated into regulations or codes tailored to each specific locality.

Surana et al. [2] undertook a survey to develop a building classification scheme specifically for structures in the Himalayan region. They categorized buildings based on various factors, including building height, materials used, slope angle, foundation type, slope retaining systems, and the presence of infill walls. Their findings indicated that pre-code buildings exhibit more pronounced effectiveness in seismic fragility analysis compared to those adhering to high code standards. Complementing this study, Singh et al. [4] investigated buildings with various configurations using bi-directional excitation. Additionally, researchers [13,14] stressed the necessity of a specialized building code for sloped terrains, arguing that the codes for flat terrains underestimate ground acceleration in sloped structures. They conducted several case studies to examine the failure patterns of buildings in hilly regions, concluding that most failures were attributable to short-column failures.

Singh et al. [6] conducted a study focusing on the impact of the Sikkim earthquake (18 September 2011) on buildings in the Sikkim region. They observed that the failure patterns in their study models closely mirrored those of the actual buildings that failed during the earthquake. Their findings highlighted that uphill columns are more vulnerable than downhill columns. Additionally, they discovered that buildings situated on sloped hills experience significantly more torsion compared to those on flat terrain, a phenomenon attributed primarily to cross-slope excitation.

Farghaly et al. [15] conducted a study on the impact of foundations on buildings located in the hilly region of Dronka Village, Egypt. Initially, the study replicated the general configuration of buildings common in Dronka Village and carried out a static analysis. The initial results indicated that the buildings were safe under static conditions. However, subsequent dynamic analysis revealed that the same buildings were prone to

failure, even with a rigid raft foundation in place. A notable observation was that shear force was significantly higher in raft foundations compared to stepped foundations. Based on these findings, the conclusion was drawn that employing stepped isolation foundations could effectively reduce the slope of a building from 60 to 45 degrees, thereby preventing wedge failure.

Welsh-Huggins et al. [16] analysed buildings with stepped configurations in Mizoram and Aizawl. The researchers found that most buildings in Aizawl were designed without considering material degradation and soil–structure interaction. They observed a specific failure pattern, characterized by a zippering failure of the base column and a shearing failure in the storeys above it, particularly the second and third storeys. The study concluded that increasing the size of the columns and using larger transverse reinforcements could shift the failure mechanism from weak storey failure to side-way failure. This shift in design approach is illustrated in Figure 2, which depicts RC buildings situated in the hilly, sloped regions of India.

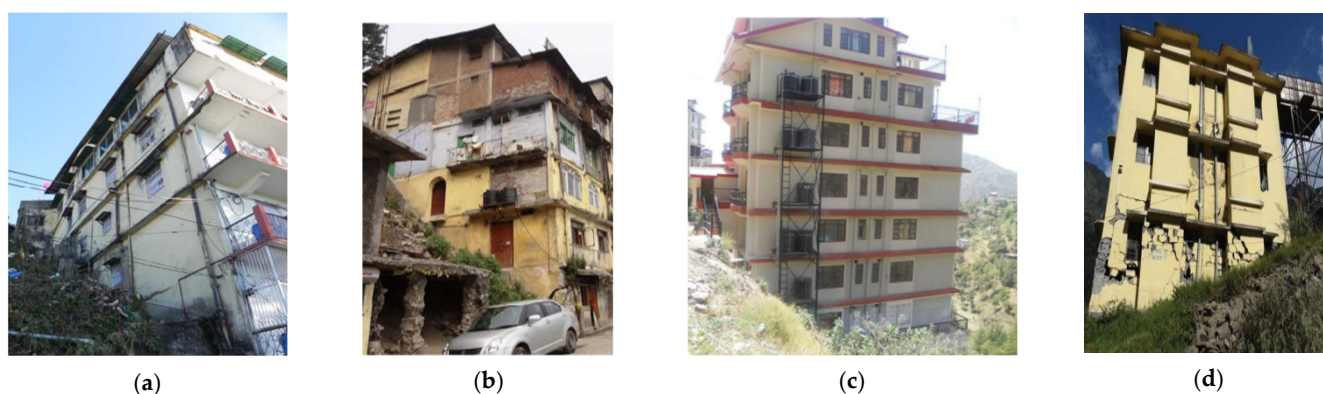


Figure 2. RC buildings situated in hilly regions of India. (a) [4], (b) [17], (c) [18], (d) [19].

3. Land Categorization

Land availability in northeast India is very limited, and most land is unfit for development. However, due to the increase in population, demand for land usage increases. Towns located in India can be categorised into four categories [20], as given in Table 1. Hilly towns in the southern regions of India such as Kerala and Tamil Nadu fall under category I and are largely exposed to sunlight and need protection from exposure to sunlight. Hilly towns from Maharashtra fall under category II. Hilly regions from the eastern part of India fall under category III as shown in Figure 3. The northern region of India falls under the last category, IV, where there is little to no sun exposure [10]. Buildings situated in towns of hilly regions of category IV (northern) are considered for the purpose of the study.

Table 1. Categories of regions across India according to latitude.

Category	Latitude	Region
I	> 14°N	Southern region of India (Kerala, Tamil Nadu, etc.)
II	14° to 22.5°	Maharashtra
III	22.5° to 28°	Eastern part of India
IV	< 28°	Northern part

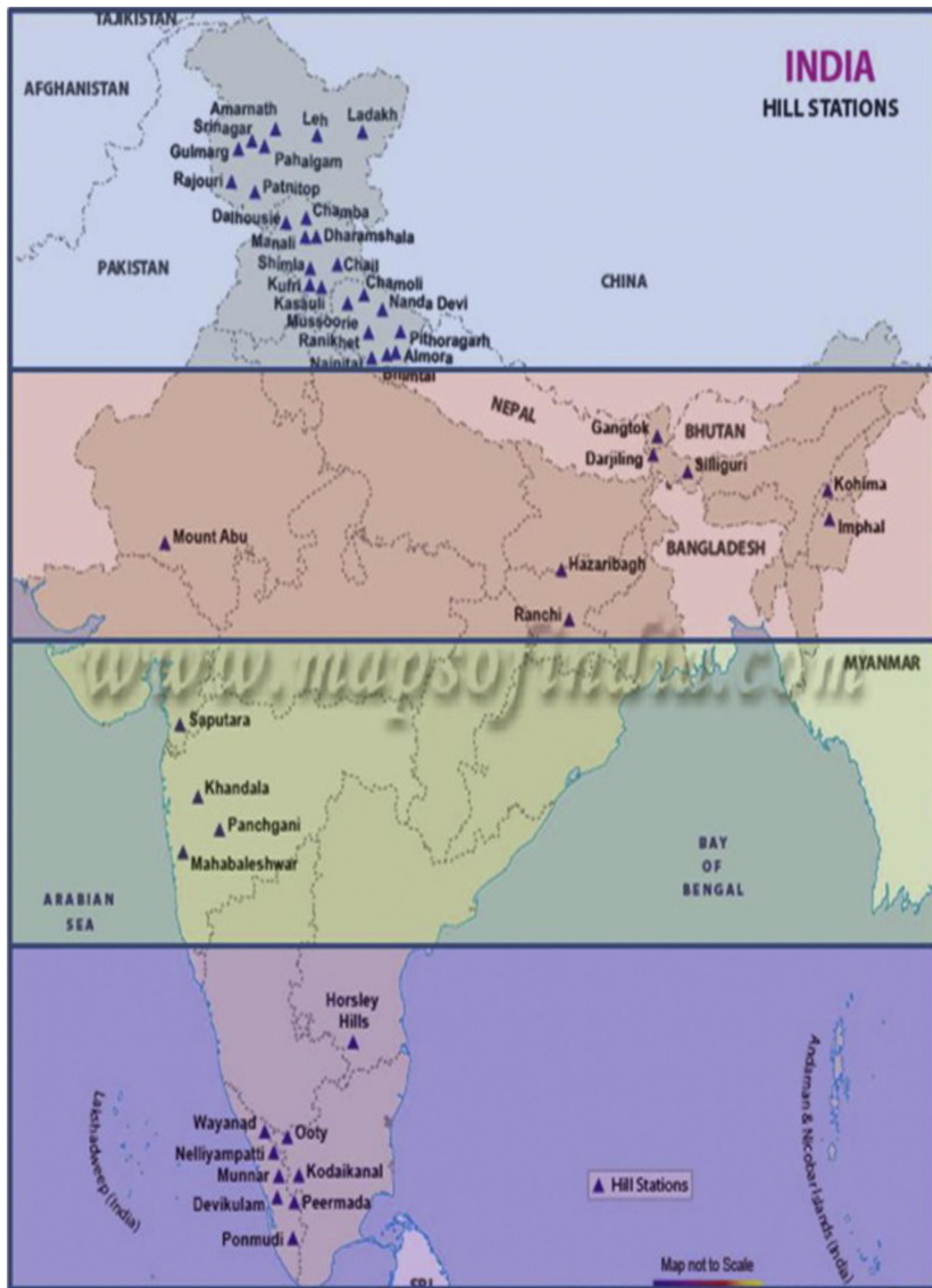


Figure 3. Hilly towns of India (<https://www.mapsofindia.com/>, (accessed on 9 November 2023)) [10].

4. Effect of the Short Column in Hilly Slope Building

Generally, in hilly slope regions, the height of the columns varies due to the sloped terrain. As the height of the columns varies, both long and short columns come into action, as shown in Figure 4b. Columns with effective lengths (lesser lateral dimension) of less than 12 are categorised as short columns [21]. When the structure is designed without any proper consideration of large forces, the column fails. Short columns are stiffer than long

columns and require more force to displace, which invariably results in short columns attracting more force, as shown in Figure 4a. Short columns have higher resistance to lateral loads compared to long columns and attract more force during earthquakes. From past research [21–24], it is found that the cracking pattern is diagonal in nature before the failure of short columns. It is technically not possible to avoid short columns due to various reasons; hence, special care in the designing of short columns has to be incorporated. IS 13920:1993 [25] recommends the usage of confining reinforcement throughout the height of the short column.

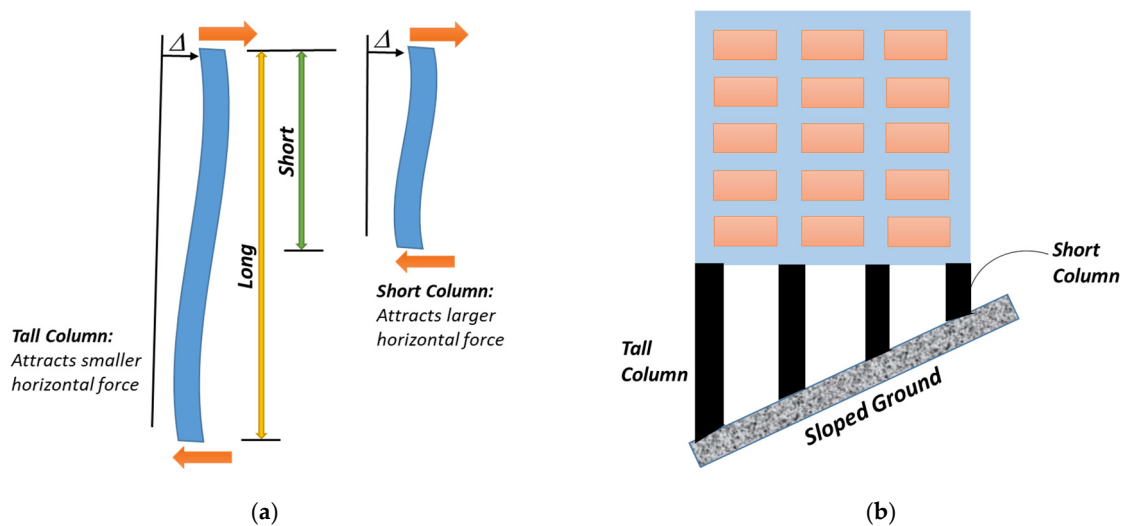


Figure 4. (a) Difference between short and long columns. (b) Representation of a building in a hilly region with a short column.

5. Effect of Infill Walls in Building

It is well known [26–29] that the strength and stiffness of RC buildings can be enhanced by using infill walls. However, many designers, while modelling and analysing RC structures, have not considered infill walls. Infill walls certainly possess stiffness and strength which can be neglected during the design of RC structures. When these parameters are not included, it can lead to an unplanned allocation of infill walls in the RC building. Usage of assumptions in design can make the design simple but may lead to serious damage to buildings during earthquakes. While designing a building for a hilly terrain, it is very important to consider all the parameters to obtain the most realistic results [30]. Past studies show that buildings with infill walls perform better in resisting lateral forces compared to those with bare frames. Ignorance of the stiffness of infill walls leads to unexpected failures due to the increased bending moment around infill walls. Also, infill walls attract a large shear force; an increase in shear force increases the storey shear of the structure. Stiff members attract larger forces, and when these stiffnesses are not included, the extent of forces attracted and their effects on RC buildings are not accounted for [26]. Brick masonry is the main constituent of infill walls and is generally weak in tension. To prevent the failure of infill walls, brick masonry has to be designed in a way that it does not carry any tension. Also, the failure of infill walls is influenced by the orientation of mortar joints. Infill walls provide a bracing effect when used in a structure, but it is very important to include the stiffness of infill walls in the design to prevent unwanted failure [26–28,31].

6. Numerical Modelling of Buildings

This study aims to understand the performance of buildings situated in hilly regions and to compare them with regular buildings on flat terrain. For this, a step-back RC building (with and without infill walls) studied on a hilly slope is compared with regular buildings of three storeys and six storeys (with and without infill walls) on flat terrain. The

regular buildings are considered as reference buildings. The step-back building is modelled as three storeys on the uphill side and six storeys on the downhill side. All three buildings have a rectangular plan, and each building plan is $10\text{ m} \times 9\text{ m}$. The details of the plan are in Figure 5a, and Figure 5b shows the sizes of beams and columns. The step-back building with and without infill walls is shown in Figure 6a–c. Regular buildings of three and six storeys with and without infill walls are shown in Figure 6d–i. The dimensions of beams and columns considered in the models are $250\text{ mm} \times 350\text{ mm}$ and $350\text{ mm} \times 350\text{ mm}$, respectively. Both roof and floor slabs have a thickness of 125 mm . Sections are designed for a compressive strength of 20 MPa , and the yield strength of steel is 415 MPa . The live loads at the roof and floor are considered as 1.5 kN/m^2 and 3 kN/m^2 ; the roof floor finish as 1 kN/m^2 . An infill wall with a thickness of 125 mm is considered for the study. All the above dimensions were determined based on the literature review. The dimensions of sections used with reinforcement are shown in Figure 5b. The dimensions considered for the study building align with most of the real buildings situated in the region of Nepal and northeast India. While designing, slabs were assumed to be rigid diaphragms, whereas 3D space frames were designed using two-node beam elements. At every nodal point, six degrees of freedom (three rotational and three translational) were assigned. The properties of the crack section were determined as per IS 1893:2016 Part 1 [20]. The current model of the building was designed in accordance with Indian standards [20,32]. In order to introduce non-linear behaviour, two plastic hinges were assigned at both ends of all the frame elements. This method is called lumped plasticity. Similarly, assignment of flexural hinges was performed on both ends of the beam. At each end of the column, hinges were assigned for axial force moment interaction (P-M-M). Hinge properties were determined according to ASCE/SEI 41-06 (2013) [33]. The modelling of the infill wall was conducted using the strut modelling procedure. Details on the modelling procedures for the strut, along with its boundary conditions, are provided in Section 6.1. Furthermore, a single-strut model was used for pushover analysis and is shown in Figure 6b,e,h. However, a cross-strut model was used for time history analysis and is shown in Figure 6c,f,i. To simulate the effect of an infill wall, axial plastic hinges were assigned at the mid-span of the strut models. All three models were designed and analysed by using non-linear analysis with the software SAP2000 v20.2.0 [8]. In such analysis, the Takeda hysteresis model is adopted to simulate hysteretic behaviour in time history analysis for all the buildings. The analysis was conducted assuming the base of the building to be fixed.

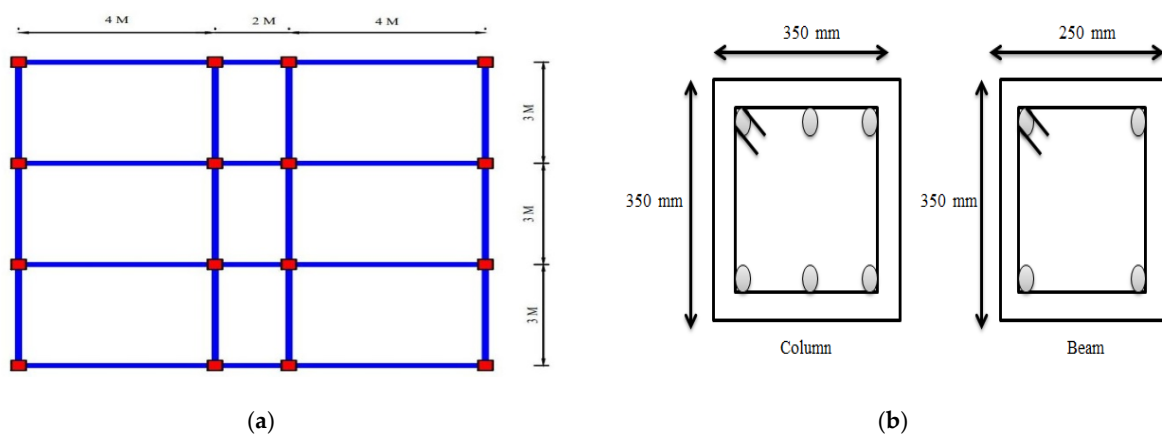


Figure 5. (a) Plan view; (b) cross-section of column and beam.

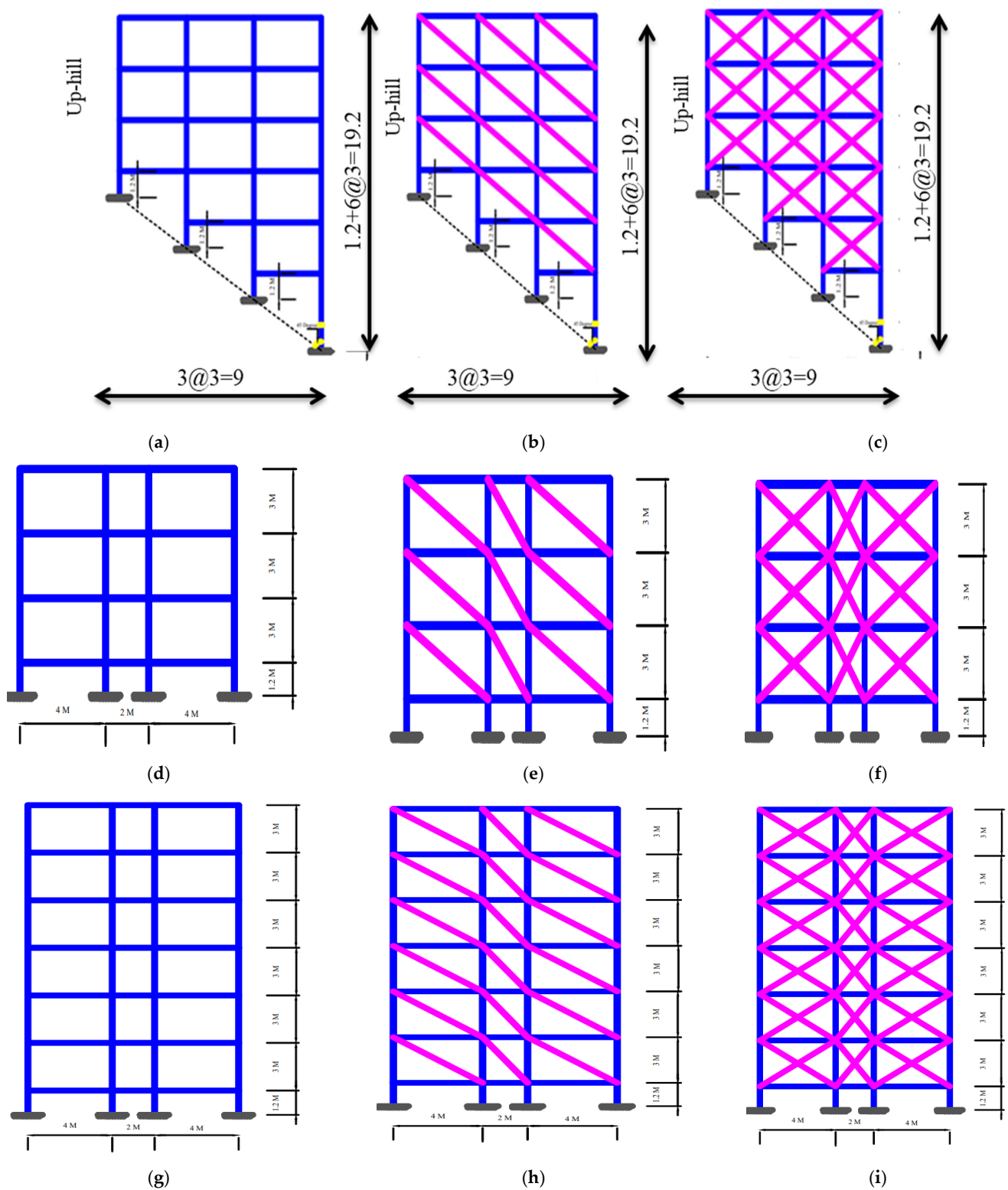


Figure 6. (a) Step-back building; (b) step-back building with single-strut infill; (c) step-back building with infill; (d) 3-storey regular building; (e) 3-storey regular building with single-strut infill; (f) 3-storey regular building with infill; (g) 6-storey regular building; (h) 6-storey regular building with single-strut infill; (i) 6-storey regular building with infill.

6.1. Modelling of Masonry Infill

To adopt the real scenario, infill walls were designed as masonry infill. The strength and elastic moduli of the masonry prism are taken from IS 1893 Part 1 [22] and are given below:

$$f_m = 0.433f_b^{0.64}f_{mo}^{0.36} \quad (1)$$

$$E_{me} = 550f_m \quad (2)$$

where f_m , f_b , f_{mo} , and E_{me} represent the compressive strength of the masonry prism, the compressive strength of the brick unit, the compressive strength of mortar, and the modulus of elasticity of brick, respectively. All the units are in Mpa. Generally, in the northeast regions, second-class bricks are used for the construction of buildings, and the compressive strengths of mortar and masonry bricks were considered in accordance with IS 1077:1992 [34]. The mortar mix ratio of cement to sand was considered to be 1:4. To simulate the stress and strain behaviour of concrete, Mander's confined concrete model was used and is shown in Figure 7b. Similarly, for steel, the elastoplastic law was adopted [35]. To include the non-linear behaviour of masonry, an idealised stress–strain curve formatted by Kaushik et al. [27] was used and is shown in Figure 7a. In this study, an infill wall of a thickness of 125 mm was considered.

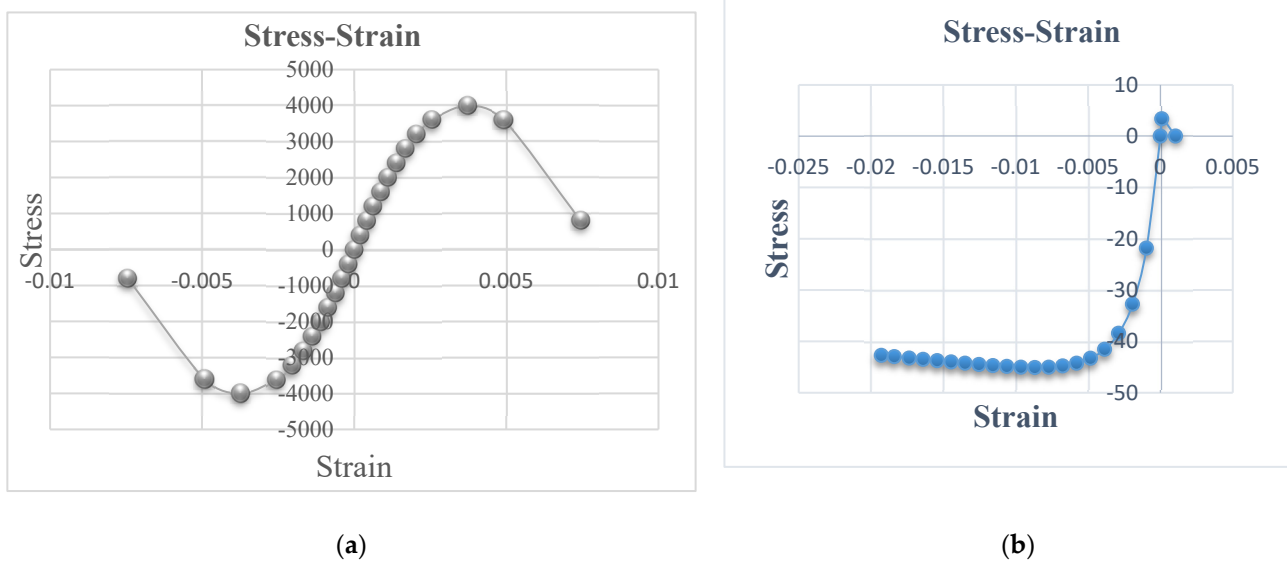


Figure 7. (a) Idealized stress–strain curve, (b) Mander confined concrete.

Diagonal struts were used to demonstrate the action of infill walls, which was done by calculating the effective width of the diagonal strut, and this is shown in Figure 8. The effective width (a) was adopted from ASCE 41 [33] and is given in Equation (3). A similar procedure is carried out in the Indian code IS 1893:2016 [20], as well as in other seismic codes of different countries.

$$a = 0.175(\lambda_1 \times h_{col})^{-0.4}r_{inf} \quad (3)$$

$$r_{inf} = \sqrt{h_{inf}^2 + L_{inf}^2} \quad (4)$$

where h_{col} is the column height (centre to centre of the beam) and r_{inf} represents the diagonal length of the infill panel. λ_1 represents the coefficient through which the effective width can be found and is given in Equation (5).

$$\lambda_1 = \left[\frac{E_{me}t_{inf} \sin 2\theta}{4E_{fe}I_{col}h_{inf}} \right]^{\frac{1}{4}} \quad (5)$$

$$I_{col} = \frac{bd^3}{12} \quad (6)$$

$$\theta = \tan^{-1} \left(\frac{h_{inf}}{L_{inf}} \right) \times \frac{\pi}{180} \quad (7)$$

where h_{inf} is the height of the infill panel; L_{inf} represents the length of the infill panel; E_{fe} and E_{me} represent the expected moduli of elasticity of the frame and infill material. I_{col} is the column's moment of inertia; t_{inf} is the thickness of the infill panel or equivalent strut; and θ is the angle made wherein the tangent is equal to the infill height-to-length aspect ratio. The expression given in Equation (8) represents the formation of plastic hinges [27].

$$l_p = 0.08L + 0.22d_b f_y \quad (8)$$

where L is the half-length of the member in meters considering the point of contra-flexure at the mid-point of the member; d_b is the diameter (in m) of the longitudinal reinforcement, and f_y is the yield strength (in MPa) of the longitudinal bars. The properties of hinges were defined using FEMA-356 [5,36]. The non-linear behaviour of the infill walls was stimulated through axial plastic hinges. The length of the plastic hinge is generally about 0.5–0.75 times the length of the strut [28]. It has been noted by many researchers that variation in the length of plastic hinges does not affect the performance of the frames [37]. For the purpose of this study, the length of the plastic hinge was taken as half the total length of the strut.

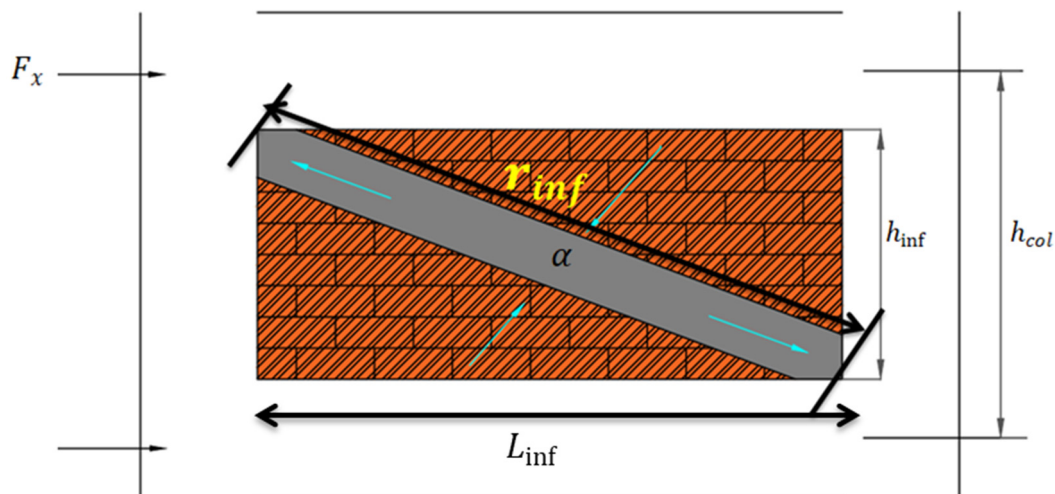


Figure 8. Equivalent diagonal strut of URM infill wall.

7. Non-Linear Analysis to Assess Capacity and Demand

This study aims to evaluate the performance of an RC building with and without infill walls situated in a hilly region. The performance of the study building is evaluated by non-linear static analysis and by non-linear dynamic analysis.

7.1. Non-Linear Static Analysis

Non-linear static analysis was performed according to the guidelines of ATC 40 [38]. Initially, pushover analysis was carried out by applying gravity loads followed by monotonically increasing the lateral load. The lateral load distribution represents the inertial force of the building, which it may experience during ground shaking. In this analysis, the parabolic load pattern was used, which represents the equivalent static load distribution along the height of the building. The global response is represented by the base shear vs. displacement curve, which is called the pushover or capacity curve. The performance point (maximum inelastic capacity of the structure) is defined as a point, where the Capacity Spectrum and the Demand Spectrum intersect for a particular damping ratio. In this study, the optimal performance parameters for the Design Basis Earthquake (DBE) and the

Maximum Considered Earthquake (MCE) were determined. According to IS 1893:2016 [20], Maximum Considered Earthquake (MCE) peak ground acceleration (PGA) for Zone V is 0.36 g, and DBE acceleration is 0.18 g, during the structure's service life [39]. Levels of damage, as shown in Figure 9a, such as immediate occupancy (IO), life safety (LS), and collapse prevention (CP), are defined according to ASCE 41-06 (2007) [33]. At the IO level, minor fractures are seen in non-structural parts of the building. Together with residual stiffness and strength in all storeys, a permanent drift is included into the structural design at the level of LS. At the level of CP, the buildings are barely stable, although the walls and columns are still functional. At this point, the building's non-structural components are severely compromised, and it is dangerously close to collapse [40]. Figure 9b highlights the various levels of damage in an RC building.

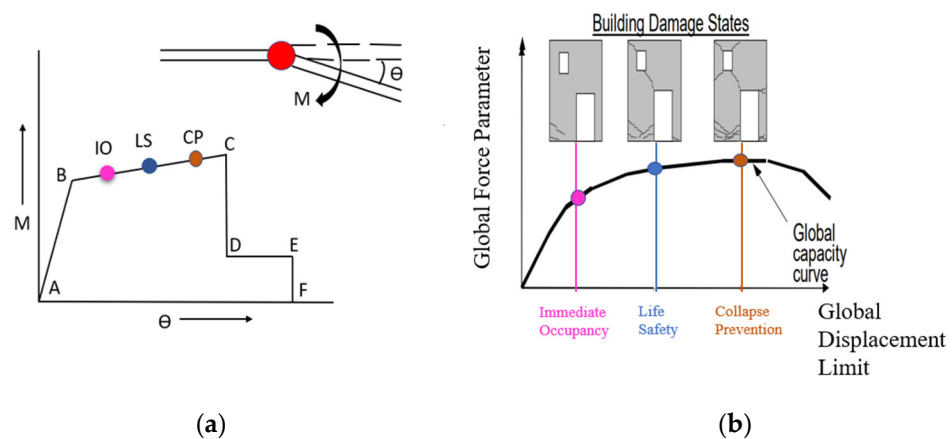


Figure 9. (a) Common flexural hinge features, (b) global capacity curve.

7.2. Non-Linear Dynamic Analysis

For the present study, a non-linear time history analysis was performed to understand the dynamic behaviour of RC buildings. A set of four far-field ground motions were used and are shown in Figure 10a–d. The earthquakes used in the study are the 1992 Big Bear earthquake (M_w 6.5), 1999 Chi-Chi earthquake (M_w 7.7), 1989 Loma Prieta earthquake (M_w 6.9), and 1994 North Ridge earthquake (M_w 6.7). These ground motion data were scaled up with the peak ground accelerations (PGAs) of 0.18 g and 0.36 g to generate the results of storey displacement and storey drift ratio. The corresponding peak ground accelerations obtained from the scale factor are given below:

$$\text{Scale Factor (S.F.)} = \frac{\text{Required PGA}}{\text{Current PGA}} \quad (9)$$

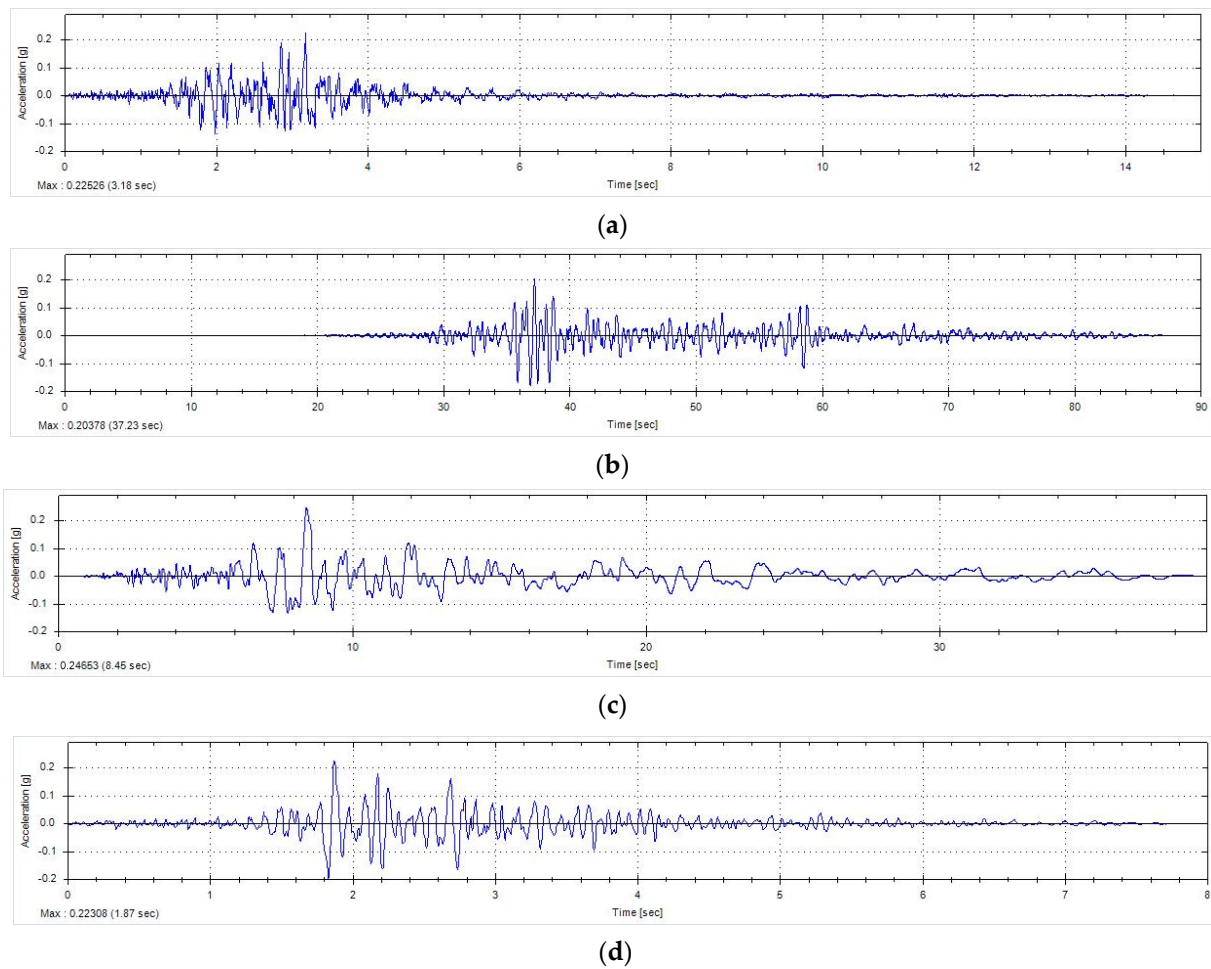


Figure 10. (a) Big Bear, (b) Chi-Chi, (c) Loma Prieta, (d) North Ridge.

Information about ground motions is shown in Table 2. The velocity of the shear wave was in the range of 180 m/s to 750 m/s, which means that the ground where the earthquake was recorded was firm. These recorded ground motions were farther than or equal to 20 km from the fault.

Table 2. Earthquake details with PGA.

S.No.	Earthquake	Date	Magnitude in Richter Scale (Mw)	PGA	S.F. (0.18 g)	S.F. (0.36 g)
1	Big Bear	28 June 1992	6.5	0.223	7.918	15.836
2	Chi-Chi	20 September 1999	7.7	0.202	8.702	17.405
3	Loma Prieta	18 October 1989	6.9	0.246	7.163	14.326
4	North Ridge	17 January 1994	6.7	0.223	7.918	15.836

8. Results and Discussion

The performance assessment of the study buildings was conducted through pushover analysis, which evaluates the capacity curve, hinge pattern, and bending moment. Meanwhile, the non-linear time history analysis provides insights into storey displacement and storey drift ratio.

8.1. Capacity Curve

This research analysed building stability through the lens of capacity curves, which graph a building's sway against its base resistance. The curves, particularly for top-floor nodes in the X and Y directions, are illustrated in Figure 11a,b. Structures with infill walls, represented by dotted lines, show greater peak base forces: 25% for step-back buildings (SBIN), 20% for three-storey (3SRIN), and 30% for six-storey (6SRIN) regular buildings compared to those without infill (SB, 3SR, and 6SR). The integration of infill walls significantly increases rigidity, enhancing lateral force resistance while reducing flexibility.

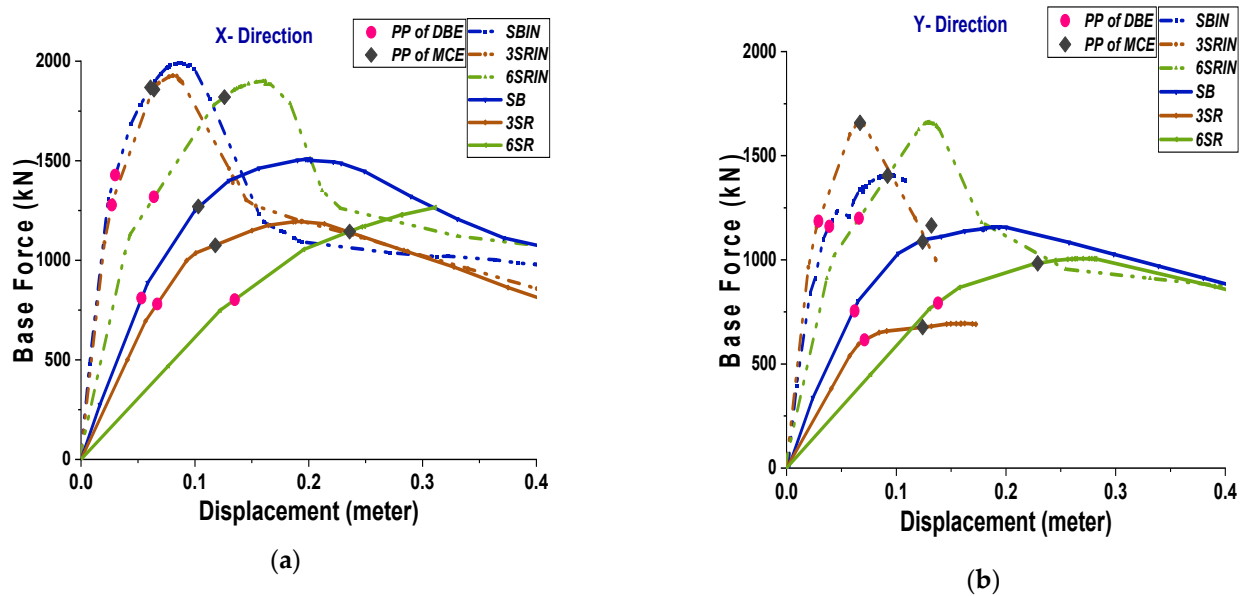


Figure 11. Capacity curves of buildings with and without infill walls in the (a) X and (b) Y directions.

The study finds that step-back buildings without infill (SB) are more vulnerable to structural component failure due to their increased flexibility and lower force absorption capacity. In contrast, step-back buildings with infill (SBIN) demonstrate less damage at the Design Basis Earthquake (DBE) level, as they meet the demand and capacity within the elastic range. However, at the Maximum Considered Earthquake (MCE) level, a distinct shift in failure mechanisms is observed. In buildings with infill walls, the damage primarily occurs within the infill walls, while in those without infill, significant frame failure is noted. This indicates a pivotal role of infill walls in altering the damage distribution under seismic loading conditions.

Figure 12 shows the hinge pattern of a step-back building in the X direction. It can be observed that the first hinge is formed in the short column because the short column attracts a large force. Further, at the DBE performance point, a total of 12 hinges are formed; this is shown in Figure 12b. Table 3a gives the details of hinge formation along the step-back building for each interval. The structural components in the uphill side of the building fall in the range of IO to LS. Hence, it is seen that the uphill side of the building is more vulnerable at the DBE level. However, at the MCE performance point, 77 hinges were formed, and are shown in Figure 12c. From Table 3a it can be seen that some of the hinges on the uphill side columns fall in the region of C to D, which concludes with the total collapse of the frame. Also, the maximum number of hinges were formed in the uphill side of the step-back building, which shows the vulnerability of step-back buildings.

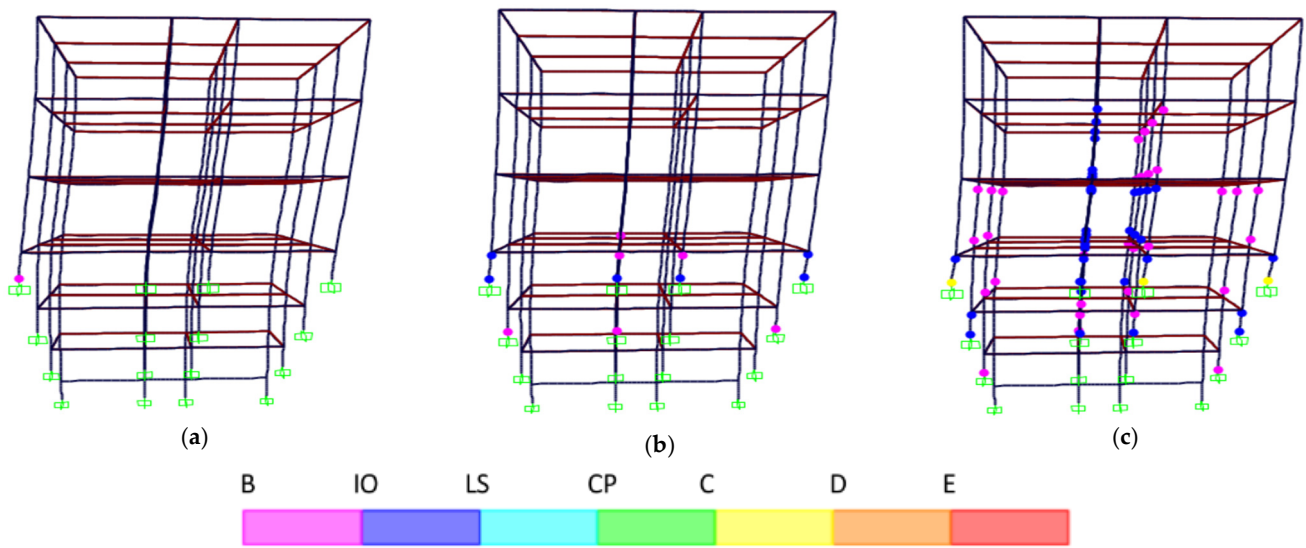


Figure 12. Hinge pattern of step-back building: pushover analysis in X direction; (a) first hinge; (b) performance point at DBE; (c) performance point at MCE.

Table 3. (a): Hinge states of step-back building (SB) without infill determined by pushover analysis in X direction; (b): hinge states of step-back building (SB) determined by pushover analysis in Y direction.

(a)											
Step	Displacement (m)	Base Force (kN)	Hinge States								Total Hinges
			A to B	B to IO	IO to LS	LS to CP	CP to C	C to D	D to E	>E	
0	3.37×10^{-6}	0	428	0	0	0	0	0	0	0	428
1	0.016508	274.949	427	1	0	0	0	0	0	0	428
2	0.058643 (Performance point of DBE)	887.488	416	6	5	1	0	0	0	0	428
3	0.100257	1252.256	378	28	20	2	0	0	0	0	428
4	0.129842 (Performance point of MCE)	1400.401	351	31	39	4	0	3	0	0	428
5	0.156239	1462.477	331	34	50	5	0	8	0	0	428
6	0.19024	1502.974	325	23	59	8	0	13	0	0	428
7	0.197378	1507.177	323	21	54	10	0	20	0	0	428
8	0.198634	1507.298	320	21	53	13	0	21	0	0	428
9	0.199333	1507.296	316	21	52	17	0	22	0	0	428
10	0.200246	1507.517	313	21	50	19	1	24	0	0	428
(b)											
Step	Displacement (m)	Base Force (kN)	Hinge States								Total Hinges
			A to B	B to IO	IO to LS	LS to CP	CP to C	C to D	D to E	>E	
0	0.001531	0	428	0	0	0	0	0	0	0	428
1	0.024014	337.8	426	2	0	0	0	0	0	0	428
2	0.065258 (Performance point of DBE)	802.381	413	10	4	1	0	0	0	0	428
3	0.101836	1030.954	374	36	16	2	0	0	0	0	428

Table 3. Cont.

(b)											
Step	Displacement (m)	Base Force (kN)	Hinge States								Total Hinges
			A to B	B to IO	IO to LS	LS to CP	CP to C	C to D	D to E	>E	
4	0.123451 (Performance point of MCE)	1095.505	361	32	28	3	0	4	0	0	428
5	0.14109	1111.587	355	24	40	5	0	4	0	0	428
6	0.162517	1137.976	349	28	40	7	0	4	0	0	428
7	0.178234	1148.085	345	24	42	11	0	6	0	0	428
8	0.179581	1150.331	345	24	40	11	0	8	0	0	428
9	0.179585	1147.076	343	24	40	13	0	8	0	0	428
10	0.180562	1150.155	340	24	38	15	1	10	0	0	428

Table 3a,b provide the details of hinges formed in a step-back building (SB) without infill walls at different intervals determined by pushover analysis in the X and Y directions. The highlighted intervals in Table 3a,b show the performance points of the DBE and MCE at their respective intervals.

Figure 13 shows the hinge pattern of a step-back building in the Y direction. Here also it is observed that the first hinge was formed in the short column due to the attraction of a large force. Further, at the DBE performance point, a total of 15 hinges were formed and are shown in Figure 13b. Table 3b gives the details of hinge formation along the step-back building for each interval. Structural components in the uphill side of the building fall in the range of IO to LS. Hence, at the MCE performance point, a total of 73 hinges were formed and are shown in Figure 13c. From Table 3b it can be seen that some of the hinges at the uphill side columns fall in the range of C to D, which concludes with the total collapse of the frame. Also, the maximum number of hinges were formed at the uphill side of the step-back building, which shows the vulnerability of step-back buildings.

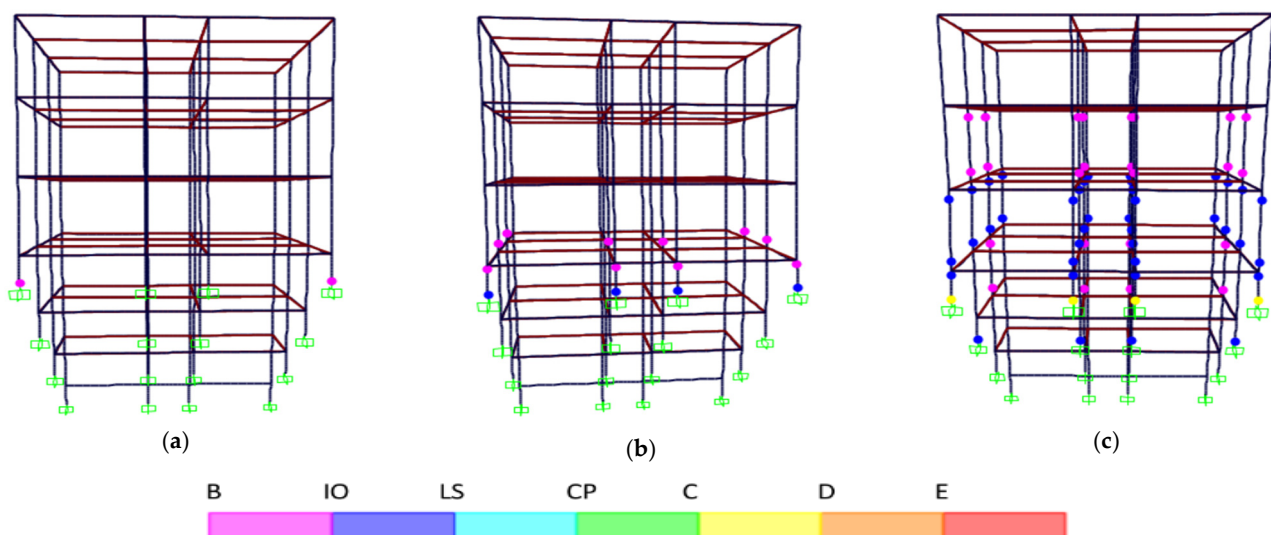


Figure 13. Hinge pattern of step-back building: pushover analysis in Y direction; (a) first hinge; (b) performance point at DBE; (c) performance point at MCE.

Figure 14 illustrates the hinge pattern in a step-back building with infill in the X direction. It has been observed that the first hinge forms in the short column, which attracts a large force. Additionally, at the Design Basis Earthquake (DBE) performance point, a

total of 21 hinges were formed, as depicted in Figure 14b. Table 4a provides detailed information about the formation of hinges along the step-back building with infill at each interval. Structural components of the uphill side of the building fall in the range of IO to LS, and the rest of the hinges formed in the infill of the building. Hence, at the DBE performance point, the uphill-side-storeys' infill walls underwent little damage that can undergo retrofitting. However, at the MCE performance point, 79 hinges were formed and are shown in Figure 14c. From Table 4a, it can be seen that some of the hinges fall in the range of LS to CP and some of them fall in the range of C to D on the uphill side of the short column. We conclude that the building underwent severe damage that cannot be retrofitted. Also, in the uphill side of the step-back building with infill, most of the infill walls underwent complete collapse.

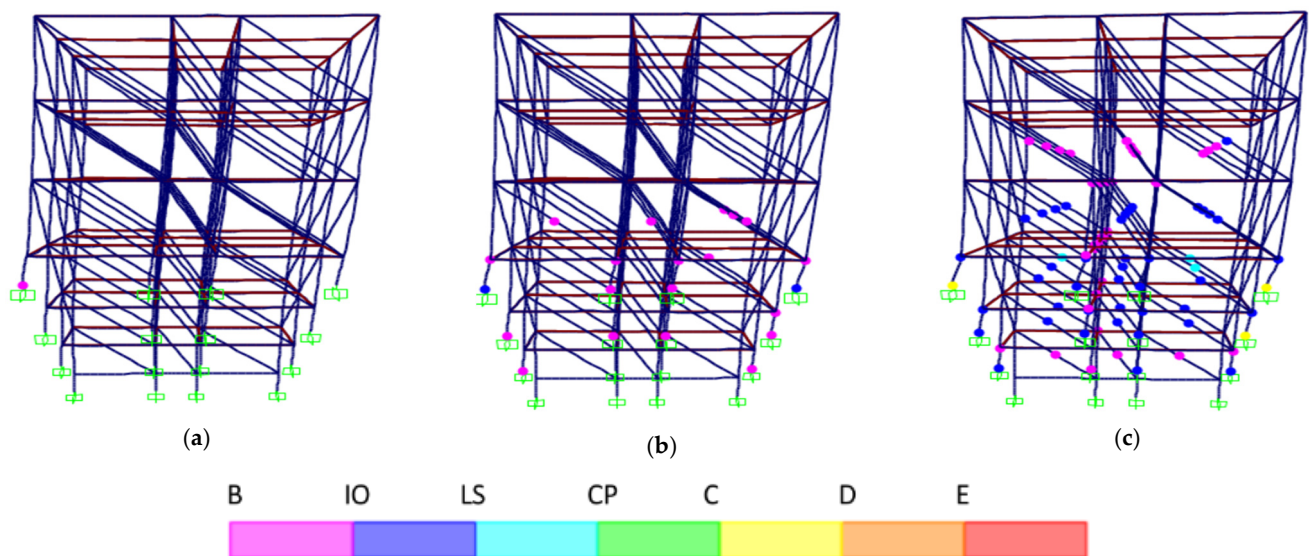


Figure 14. Hinge pattern of step-back building with infill: pushover analysis in X direction; (a) first hinge; (b) performance point at DBE; (c) performance point at MCE.

Table 4. (a): Hinge states of step-back building with infill (SBIN) determined by pushover analysis in X direction, (b): hinge states of step-back building with infill (SBIN) determined by pushover analysis in Y direction.

(a)											
Step	Displacement (m)	Base Force (kN)	Hinge States								Total Hinges
			A to B	B to IO	IO to LS	LS to CP	CP to C	C to D	D to E	>E	
0	−0.00051	0	530	0	0	0	0	0	0	0	530
1	0.007504	481.395	529	1	0	0	0	0	0	0	530
2	0.023899 (Performance point of DBE)	1308.51	509	19	2	0	0	0	0	0	530
3	0.043738	1683.536	480	15	34	1	0	0	0	0	530
4	0.051811	1778.421	466	23	39	2	0	0	0	0	530
5	0.052207	1780.829	466	23	38	2	0	1	0	0	530
6	0.064809 (Performance point of MCE)	1901.52	451	33	40	3	0	3	0	0	530

Table 4. Cont.

(a)											
Step	Displacement (m)	Base Force (kN)	Hinge States								Total Hinges
			A to B	B to IO	IO to LS	LS to CP	CP to C	C to D	D to E	>E	
7	0.070087	1938.692	444	36	41	3	0	6	0	0	530
8	0.07514	1967.581	441	38	38	5	0	8	0	0	530
9	0.075977	1970.606	441	38	38	5	0	8	0	0	530
10	0.075977	1970.61	441	38	38	4	0	9	0	0	530
(b)											
0	0.001113	0	530	0	0	0	0	0	0	0	530
1	0.008974	393.359	529	1	0	0	0	0	0	0	530
2	0.021334 (Performance point of DBE)	838.81	518	8	4	0	0	0	0	0	530
3	0.039607	1173.391	494	24	12	0	0	0	0	0	530
4	0.046294	1237.276	486	25	18	1	0	0	0	0	530
5	0.056676	1207.96	486	16	25	2	0	1	0	0	530
6	0.06901	1348.26	480	16	26	2	0	6	0	0	530
7	0.072464	1354.072	479	8	30	3	0	10	0	0	530
8	0.084239	1397.814	471	11	32	4	0	12	0	0	530
9	0.089828 (Performance point of MCE)	1404.564	454	12	30	20	0	14	0	0	530
10	0.094566	1404.501	451	10	32	22	0	15	0	0	530

Table 4a,b show the details of hinges formed in a step-back building with infill (SBIN) at different intervals determined by pushover analysis in both X and Y directions. The highlighted intervals in Table 4a,b show the performance points of the DBE and MCE at their respective intervals.

Figure 15 shows the hinge pattern of a step-back building with infill in the Y direction. It can be observed that the first hinge was formed in the short column because the short column attracts a large force. Furthermore, at the DBE performance point, a total of 12 hinges were formed and are shown in Figure 15b. Table 4b gives the details of hinge formation along the step-back building without infill for each interval. Structural components in the uphill side of the building fall in the range of IO to LS, and the rest of the hinges fall in the infill of the building. Hence, at the DBE level, only short columns underwent deformation, and no damage was observed in infill walls. However, at the MCE performance point, 76 hinges were formed and are shown in Figure 15c. From Table 4b, it can be seen that the hinges were formed at infill walls in the range of the IO to LS levels, and some of the hinges on short columns fall in the range of C to D, from which we conclude that the step-building with infill underwent severe damage at the MCE performance point.

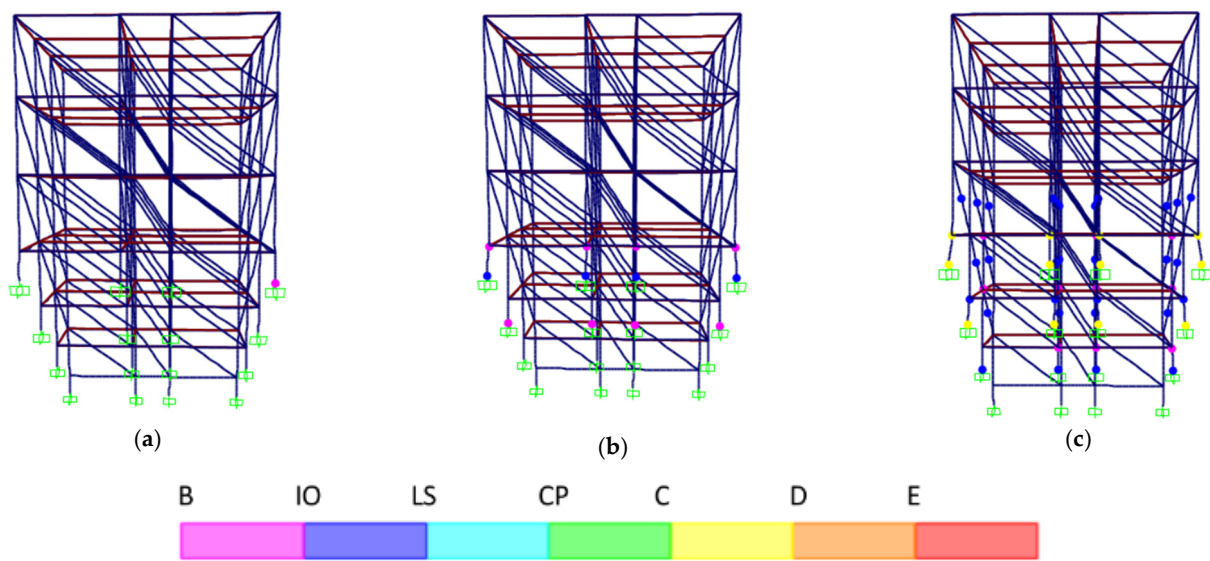


Figure 15. Hinge pattern of step-back building with infill: pushover analysis in Y direction; (a) first hinge; (b) performance point at DBE; (c) performance point at MCE.

Figure 16 shows the hinge pattern of a three-storey regular building in the X direction. It can be observed that the first hinge was formed at an intermediate column of the building. Further, at the DBE performance point, a total of two hinges were formed and are shown in Figure 16b. Table 5a gives the details of hinge formation along the three-storey regular building for each interval. Structural components in the intermediate column of the building fall in the range of B to IO. Hence, it can be seen that a three-storey regular building does not undergo deformation. However, at the MCE performance point, 48 hinges were formed and are shown in Figure 16c. From Table 5a, it can be seen that few hinges on intermediate columns fall in the range of IO to LS, from which we conclude that the three-storey regular building shows moderate damage and can be retrofitted.

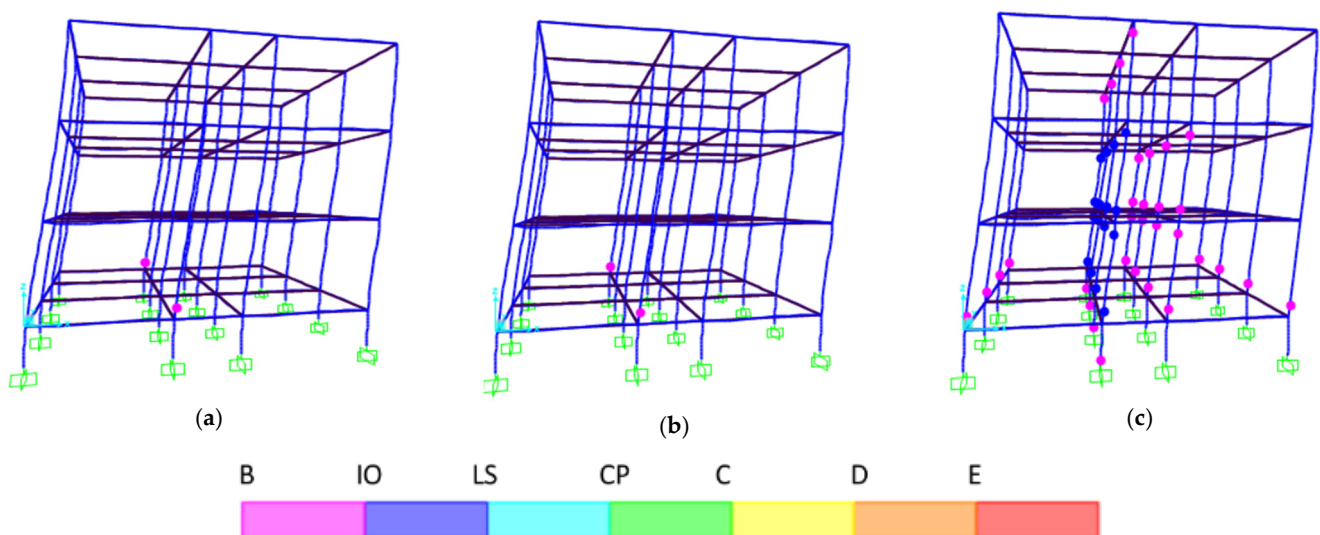


Figure 16. Hinge pattern of 3-storey regular building: pushover analysis in X direction; (a) first hinge; (b) performance point at DBE; (c) performance point at MCE.

Table 5a,b show the details of hinges formed in three-storey regular buildings (3SRs) without infill walls at different intervals determined by pushover analysis in the X and Y directions. The highlighted intervals in Table 5a,b show the performance points of the DBE and MCE at their respective intervals.

Table 5. (a): Hinge states of 3-storey regular building (3SR) determined by pushover analysis in X direction, (b): hinge states of 3-storey regular building (3SR) determined by pushover analysis in Y direction.

(a)											
Step	Displacement (m)	Base Force (kN)	Hinge States								Total Hinges
			A to B	B to IO	IO to LS	LS to CP	CP to C	C to D	D to E	>E	
0	3.29×10^{-6}	0	320	0	0	0	0	0	0	0	320
1	0.040803	500.151	320	0	0	0	0	0	0	0	320
2	0.056657 (Performance point of DBE)	694.491	318	2	0	0	0	0	0	0	320
3	0.092746	998.665	286	18	16	0	0	0	0	0	320
4	0.100759 (Performance point of MCE)	1036.97	272	32	16	0	0	0	0	0	320
5	0.150091	1149.05	258	14	48	0	0	0	0	0	320
6	0.164534	1176.15	244	28	48	0	0	0	0	0	320
7	0.186342	1193.17	242	22	48	0	0	8	0	0	320
8	0.188357	1194.2	242	22	46	0	0	10	0	0	320
9	0.193378	1195.16	242	22	42	0	0	14	0	0	320
10	0.213778	1183.07	242	22	32	0	0	24	0	0	320

(b)											
Step	Displacement (m)	Base Force (kN)	Hinge States								Total Hinges
			A to B	B to IO	IO to LS	LS to CP	CP to C	C to D	D to E	>E	
0	7.69×10^{-7}	0	320	0	0	0	0	0	0	0	320
1	0.040801	381.97	320	0	0	0	0	0	0	0	320
2	0.05749	538.22	316	4	0	0	0	0	0	0	320
3	0.065447	593.82	288	32	0	0	0	0	0	0	320
4	0.069831 (Performance point of DBE)	612.19	280	40	0	0	0	0	0	0	320
5	0.084261	650.68	270	34	16	0	0	0	0	0	320
6	0.091297 (Performance point of MCE)	658.12	264	32	24	0	0	0	0	0	320
7	0.132097	680.98	264	14	42	0	0	0	0	0	320
8	0.145848	691.13	264	8	34	0	0	14	0	0	320
9	0.149734	692.75	264	8	28	0	0	20	0	0	320
10	0.15458	693.61	264	8	26	0	0	22	0	0	320

Figure 17 shows the hinge pattern of a three-storey regular building in the Y direction. It can be observed that the first hinge was formed at the intermediate column of the building. Furthermore, at the DBE performance point, a total of 40 hinges were formed and are shown in Figure 17b. Table 5b gives the details of hinge formation along the three-storey regular building for each interval. Structural components at the first and second storeys of the building fall in the range of B to IO. Hence, it can be seen that a three-storey regular building does not undergo deformation. However, at the MCE performance point, 56 hinges were formed and are shown in Figure 17c. From Table 5b, it can be seen that some of the hinges at the first storey of the building fall in the range of IO to LS, from which

we conclude that the three-storey regular building shows moderate damage and can be retrofitted.

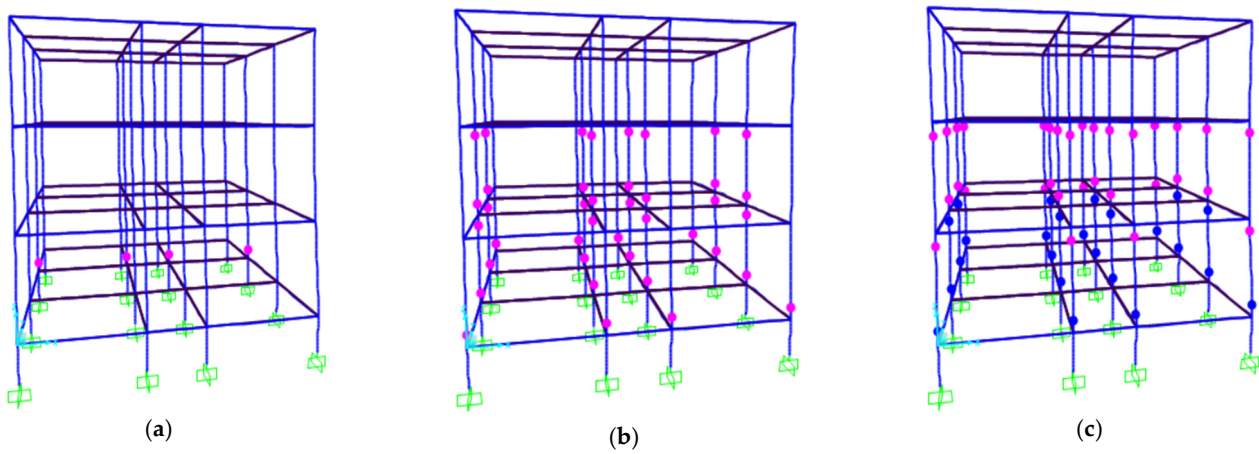


Figure 17. Hinge pattern of 3-storey regular building: pushover analysis in Y direction; (a) first hinge; (b) performance point at DBE; (c) performance point at MCE.

Figure 18 shows the hinge pattern of a three-storey regular building with infill in the X direction. It can be observed that the first hinge was formed at intermediate infill walls of the building. Furthermore, at the DBE performance point, a total of two hinges were formed and are shown in Figure 18b. Table 6a gives the details of hinge formation along the three-storey regular building with infill for each interval. Structural components in infill walls of the building fall in the range of B to IO. Hence, it can be seen that a three-storey regular building with infill does not undergo deformation. However, at the MCE performance point, 55 hinges were formed and are shown in Figure 18c. From Table 6a, it can be seen that in infill walls of the building, some hinges fall in the range of LS to CP and some fall in the range of C to D, from which we conclude that there was a total collapse of infill walls at the first storey of the building.

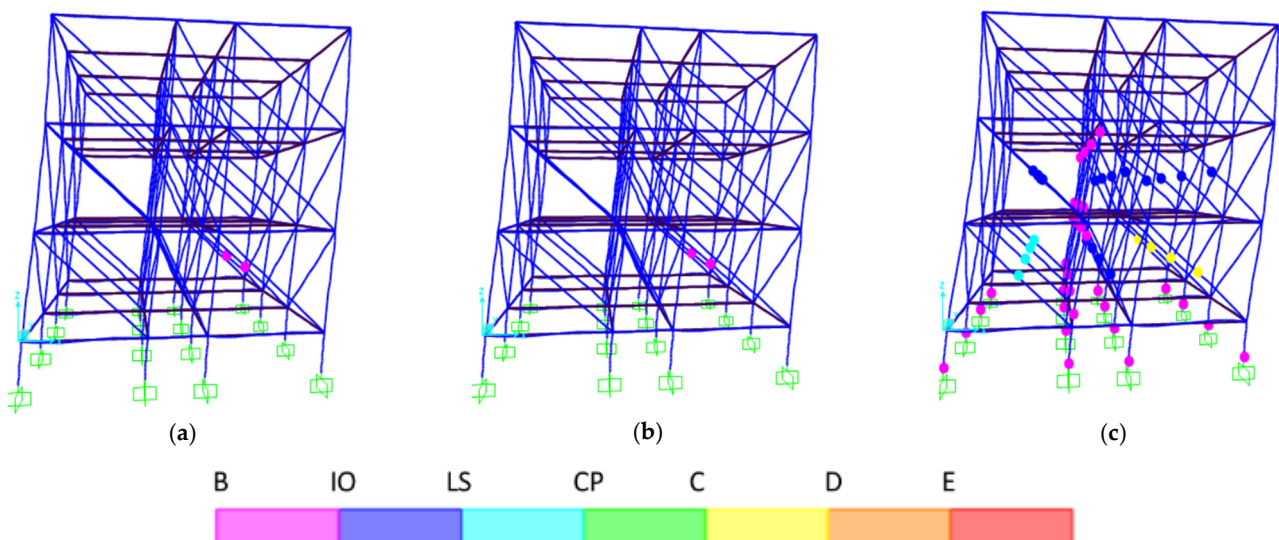


Figure 18. Hinge pattern of 3-storey regular building with infill: pushover analysis in X direction; (a) first hinge; (b) performance point at DBE; (c) performance point at MCE.

Table 6a,b show the details of hinges formed in a three-storey regular building with infill (3SRIN) at different intervals determined by pushover analysis in the X and Y direc-

tions. The highlighted intervals in Table 6a,b show the performance points of the DBE and MCE at their respective intervals.

Table 6. (a): Hinge states of 3-storey regular building with infill (3SRIN) determined by pushover analysis in X direction, (b): hinge states of 3-storey regular building with infill (3SRIN) determined by pushover analysis in Y direction.

(a)											
Hinge States											
Step	Displacement (m)	Base Force (kN)	A to B	B to IO	IO to LS	LS to CP	CP to C	C to D	D to E	>E	Total Hinges
0	−0.00043	0	392	0	0	0	0	0	0	0	392
1	0.020552 (Performance point of DBE)	1088.78	390	2	0	0	0	0	0	0	392
2	0.027718	1300.22	368	21	3	0	0	0	0	0	392
3	0.062047 (Performance point of MCE)	1845.2	337	31	16	4	0	4	0	0	392
4	0.066487	1881.17	324	44	16	0	0	8	0	0	392
5	0.068366	1891.19	320	48	16	0	0	8	0	0	392
6	0.077247	1922.23	318	42	12	8	0	12	0	0	392
7	0.080617	1927.64	312	48	12	8	0	12	0	0	392
8	0.084141	1925.69	308	46	18	8	0	12	0	0	392
9	0.085712	1910.66	308	40	24	8	0	12	0	0	392
10	0.085981	1909.41	308	38	26	8	0	12	0	0	392
(b)											
Hinge States											
Step	Displacement (m)	Base Force (kN)	A to B	B to IO	IO to LS	LS to CP	CP to C	C to D	D to E	>E	Total Hinges
0	−0.0005	0	392	0	0	0	0	0	0	0	392
1	0.019838	964.4	388	4	0	0	0	0	0	0	392
2	0.027304 (Performance point of DBE)	1157.2	369	23	0	0	0	0	0	0	392
3	0.057731	1601.9	328	40	24	0	0	0	0	0	392
4	0.063953	1653.3	326	48	18	0	0	0	0	0	392
5	0.064059 (Performance point of MCE)	1653.7	323	48	17	0	0	4	0	0	392
6	0.064076	1653.9	324	48	16	0	0	4	0	0	392
7	0.064846	1656.5	314	48	14	0	0	6	0	0	392
8	0.065964	1658.5	320	48	12	0	0	10	0	0	392
9	0.06999	1656.1	320	52	12	0	0	14	0	0	392
10	0.06999	1656.1	312	52	12	0	0	16	0	0	392

Figure 19 shows the hinge pattern of a three-storey regular building with infill in the Y direction. It can be observed that the first hinge was formed at the intermediate infill walls of the building. Furthermore, at the DBE performance point, a total of 23 hinges were formed and are shown in Figure 19b. Table 6b gives the details of hinge formation along the three-storey regular building with infill for each interval. Structural components in the outer infill walls of the first and second storeys of the building fall in the range of B to IO. Hence, it can be seen that a three-storey regular building with infill does not undergo

deformation. However, at the MCE performance point, 69 hinges were formed in the first and second storeys of the building, which is shown in Figure 19c. From Table 6b, it can be seen that in the infill walls of the building, some hinges fall in the range of LS to CP and some fall in the range of C to D, from which we conclude that there was a collapse of infill walls at the first storey of the building.

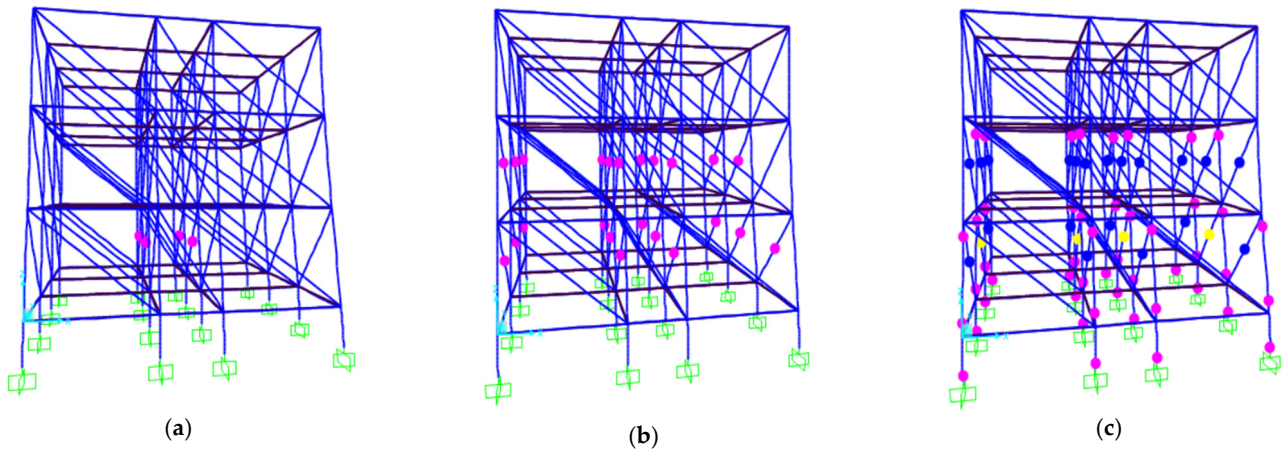


Figure 19. Hinge pattern of 3-storey regular building with infill: pushover analysis in Y direction; (a) first hinge; (b) performance point at DBE; (c) performance point at MCE.

Figure 20 shows the hinge pattern of a six-storey regular building in the X direction. It can be observed that the first hinge was formed at an intermediate column of the building. Furthermore, at the DBE performance point, a total of two hinges were formed and are shown in Figure 20b. Table 7a gives the details of hinge formation along the six-storey regular building for each interval. Structural components in the intermediate columns of the building fall in the range of B to IO. Hence, it can be seen that six-storey regular buildings do not undergo deformation. However, at the MCE performance point, 90 hinges were formed and are shown in Figure 20c. From Table 7a, it can be seen that few hinges on intermediate columns fall in the range of IO to LS, and two hinges fall in the range of LS to CP of the first storey of the building, from which we conclude that there was severe damage to the column where hinges fall in the range of LS to CP, and that the rest of the columns can be retrofitted.

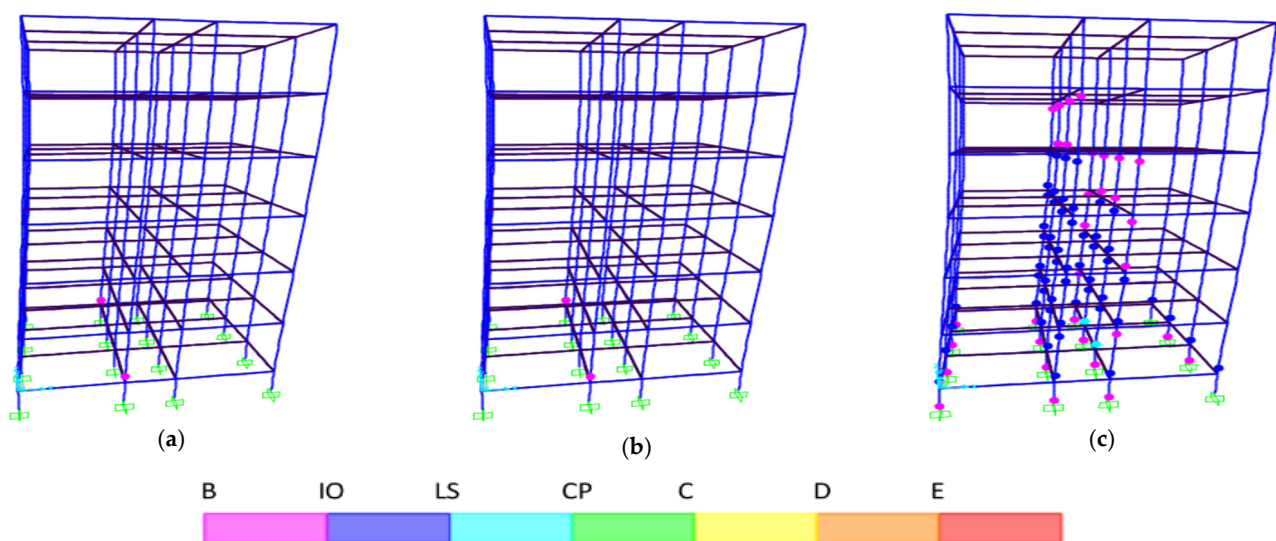


Figure 20. Hinge pattern of 6-storey regular building: pushover analysis in X direction; (a) first hinge; (b) performance point at DBE; (c) performance point at MCE.

Table 7. (a): Hinge states of 6-storey regular building (6SR) determined by pushover analysis in X direction, (b): hinge states of 6-storey regular building (6SR) determined by pushover analysis in Y direction.

(a)											
Step	Displacement (m)	Base Force (kN)	Hinge States								Total Hinges
			A to B	B to IO	IO to LS	LS to CP	CP to C	C to D	D to E	>E	
0	3.59×10^{-6}	0	560	0	0	0	0	0	0	0	560
1	0.076804	470.729	560	0	0	0	0	0	0	0	560
2	0.122233 (Performance point of DBE)	749.18	558	2	0	0	0	0	0	0	560
3	0.195619	1054.878	494	40	26	0	0	0	0	0	560
4	0.246328 (Performance point of MCE)	1168.052	470	32	56	2	0	0	0	0	560
5	0.248913	1170.758	468	34	56	2	0	0	0	0	560
6	0.280812	1227.523	462	32	58	4	0	4	0	0	560
7	0.28179	1227.964	462	32	56	4	0	6	0	0	560
8	0.311089	1265.052	443	44	56	5	0	12	0	0	560
9	0.321085	1267.062	438	46	58	6	0	12	0	0	560
10	0.351806	1268.056	423	46	58	6	12	14	0	0	560

(b)											
Step	Displacement (m)	Base Force (kN)	Hinge States								Total Hinges
			A to B	B to IO	IO to LS	LS to CP	CP to C	C to D	D to E	>E	
0	1.71×10^{-6}	0	560	0	0	0	0	0	0	0	560
1	0.076802	450.902	560	0	0	0	0	0	0	0	560
2	0.13044 (Performance point of DBE)	765.818	554	6	0	0	0	0	0	0	560
3	0.157411	866.985	496	64	0	0	0	0	0	0	560
4	0.224145 (Performance point of MCE)	978.573	450	54	56	0	0	0	0	0	560
5	0.244898	997.111	432	58	64	0	0	6	0	0	560
6	0.255741	1002.232	430	56	62	0	0	12	0	0	560
7	0.25958	1003.365	430	54	64	0	0	12	0	0	560
8	0.26229	1004.669	430	52	64	0	0	14	0	0	560
9	0.264263	1005.151	430	52	62	0	0	16	0	0	560
10	0.269726	1005.653	430	52	58	0	0	20	0	0	560

Table 7a,b show the details of hinges formed in six-storey regular building (6SR) without infill walls at different intervals determined by pushover analysis in the X and Y directions. The highlighted intervals in Table 7a,b show the performance points of the DBE and MCE at their respective intervals.

Figure 21 shows the hinge pattern of a six-storey regular building in the Y direction. It can be observed that the first hinge was formed at an intermediate column of the building. Furthermore, at the DBE performance point, a total of six hinges were formed and are shown in Figure 21b. Table 7b gives the details of hinge formation along the six-storey regular building for each interval. Structural components of the building fall in the range of B to IO. Hence, it can be seen that a six-storey regular building does not undergo deformation. However, at the MCE performance point, 110 hinges were formed and are shown in Figure 21c.

From Table 7b, it can be seen that some of the hinges from the first storey to the fourth storey of the building fall in the range of IO to LS, from which we conclude that the six-storey regular building shows moderate damage and can be retrofitted.

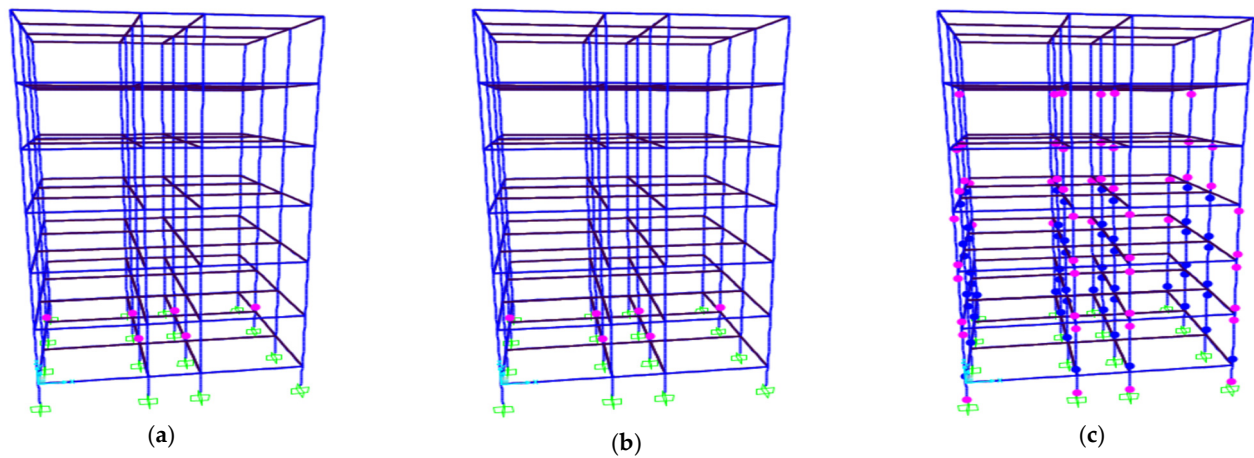


Figure 21. Hinge pattern of 6-storey regular building: pushover analysis in Y direction; (a) first hinge; (b) performance point at DBE; (c) performance point at MCE.

Figure 22 shows the hinge pattern of a six-storey regular building with infill in the X direction. It can be observed that the first hinge was formed at the intermediate infill walls of the building. Furthermore, at the DBE performance point, a total of 25 hinges were formed and are shown in Figure 22b. Table 8a gives the details of hinge formation along the six-storey regular building with infill for each interval. Structural components in the infill walls of the building fall in the range of B to IO. Hence, it can be seen that a six-storey regular building with infill does not undergo deformation. However, at the MCE performance point, 77 hinges were formed and are shown in Figure 22c. From Table 8a it can be seen that at the third storey and fourth storey of the building, hinges fall in the range of IO to LS, while at the first storey and second storey of the building, hinges fall in the range of LS to CP, and in infill walls, some hinges fall in the range of C to D, from which we conclude that the infill walls of the first and second storeys of the building show severe damage.

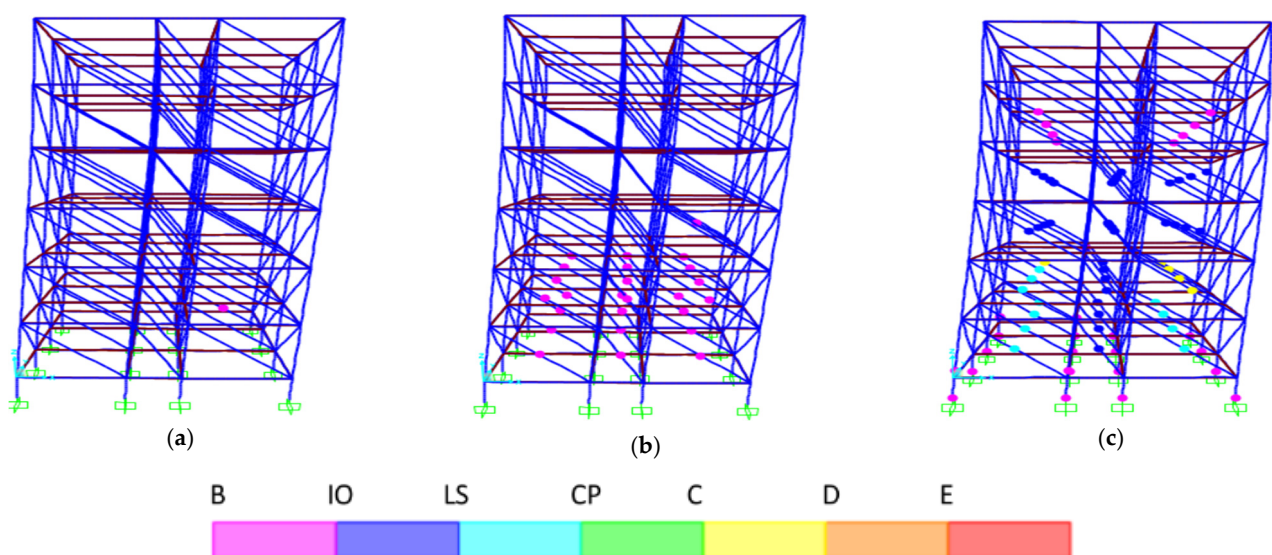


Figure 22. Hinge pattern of 6-storey regular building with infill: pushover analysis in X direction; (a) first hinge; (b) performance point at DBE; (c) performance point at MCE.

Table 8. (a): Hinge states of 6-storey regular building with infill (6SRIN) determined by pushover analysis in X direction, (b): hinge states of 6-storey regular building with infill (6SRIN) determined by pushover analysis in Y direction.

(a)											
Step	Displacement (m)	Base Force (kN)	Hinge States								Total Hinges
			A to B	B to IO	IO to LS	LS to CP	CP to C	C to D	D to E	>E	
0	−0.00169	0	704	0	0	0	0	0	0	0	704
1	0.038483	1038.003	703	1	0	0	0	0	0	0	704
2	0.043069 (Performance point of DBE)	1130.294	679	25	0	0	0	0	0	0	704
3	0.116699 (Performance point of MCE)	1780.111	627	29	32	11	0	5	0	0	704
4	0.134013	1854.465	606	46	28	7	0	17	0	0	704
5	0.134326	1855.281	606	46	28	7	0	17	0	0	704
6	0.134407	1855.689	606	46	28	6	0	18	0	0	704
7	0.135023	1857.411	606	46	28	6	0	18	0	0	704
8	0.135038	1857.485	606	46	28	5	0	19	0	0	704
9	0.136646	1861.996	605	47	28	5	0	19	0	0	704
10	0.136695	1862.236	605	47	28	4	0	20	0	0	704
(b)											
Step	Displacement (m)	Base Force (kN)	Hinge States								Total Hinges
			A to B	B to IO	IO to LS	LS to CP	CP to C	C to D	D to E	>E	
0	−0.00193	0	704	0	0	0	0	0	0	0	704
1	0.036772	912.182	703	1	0	0	0	0	0	0	704
2	0.043345 (Performance point of DBE)	1020.269	673	31	0	0	0	0	0	0	704
3	0.127187	1657.198	601	68	35	0	0	0	0	0	704
4	0.129456	1659.744	584	71	37	0	0	12	0	0	704
5	0.130397 (Performance point of MCE)	1655.252	578	73	37	2	0	14	0	0	704
6	0.130452	1655.357	560	73	39	2	0	16	0	0	704
7	0.131011	1655.734	553	73	39	3	0	22	0	0	704
8	0.131696	1655.612	547	73	41	3	0	23	0	0	704
9	0.13335	1654.003	540	75	41	5	0	26	0	0	704
10	0.134342	1652.219	555	527	43	7	0	28	0	0	704

Table 8a,b show the details of hinges formed in a six-storey regular building with infill (6SRIN) at different intervals determined by pushover analysis in the X and Y directions. The highlighted intervals in Table 8a,b show the performance points of the DBE and MCE at their respective intervals.

Figure 23 shows the hinge pattern of a six-storey regular building with infill in the Y direction. It can be observed that the first hinge was formed at the intermediate infill walls of the building. Furthermore, at the DBE performance point, a total of 31 hinges were formed and are shown in Figure 23b. Table 8b gives the details of hinge formation along the six-storey regular building with infill for each interval. Structural components in the infill walls of the building fall in the range of B to IO. Hence, it can be seen that a

six-storey regular building with infill does not undergo deformation. However, at the MCE performance point, 126 hinges were formed and are shown in Figure 23c. From Table 8b, it can be seen that, in infill walls of the first storey and second storey of the building, some of hinges fall in the range of C to D, from which we conclude that there is severe damage in the infill walls of the first and second storeys of the building.

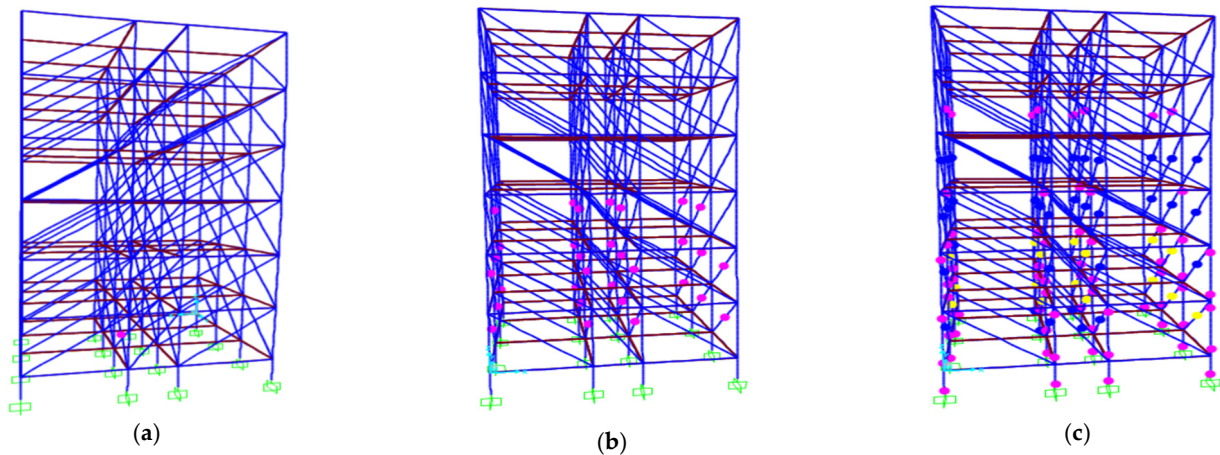


Figure 23. Hinge pattern of 6-storey regular building with infill: pushover analysis in Y direction; (a) first hinge; (b) performance point at DBE; (c) performance point at MCE.

From the observed results of the study buildings, it can be stated that most of the damage is observed in the top three storeys. The building with step-back configuration failed at the uppermost level, with the failure being due to shearing failure in a short column. The uppermost columns are rigid and they exceed the collapse limit state. The same observation can be found in the Nepal building shown in Figure 1. The hinge patterns shown in the above Figures 10–21 indicate that hinges formed in the top three storeys develop a mechanism indicating collapse. Flexural failure at the downhill region occurred due to the columns' flexibility. The hinges formed in the regular buildings were different from the hinges formed in the step-back buildings.

Table 9 shows a summary of the above-observed hinge formation. When comparing the step-back building to the three-storey and six-storey regular buildings, the first hinge is seen in a short column of the step-back building, whereas in regular buildings, the first hinge is seen in an intermediate column. Further, at the DBE performance point, the sequence of hinge formation in the step-back building starts with a short column (short columns of 1.2 m are provided to maintain the slope from ground level), followed by outer and intermediate columns. However, in regular buildings, hinges are seen only in intermediate columns due to the distribution of forces. Regarding the hinges seen in both the step-back building with infill and the step-back building without infill, the first hinge and performance point of the DBE were the same, and it can be observed that this cannot be justified by just the DBE. For the same purpose, study on hinge formation at performance points of the MCE is necessary. It can be seen that, in the step-back building with infill, hinges are seen in short columns, followed by infill walls. However, in the step-back building without infill, the hinge pattern seen starts in short columns, followed by the outer and intermediate columns. We conclude that the step-back building with infill gives better performance (in terms of storey displacement and storey drift ratio) than the step-back building without infill walls in hill regions, and a step-back building is more vulnerable than a regular building.

Table 9. Summary of hinge observations.

Building Configuration	First Hinge				Performance Point of DBE				Performance Point of MCE			
	SC	OC	IC	IN	SC	OC	IC	IN	SC	OC	IC	IN
SB-X	✓				✓				✓	✓	✓	
SB-Y	✓				✓	✓	✓		✓	✓	✓	
SBIN-X	✓				✓			✓	✓		✓	✓
SBIN-Y	✓				✓				✓			✓
3SR-X			✓				✓		✓	✓	✓	
3SR-Y			✓			✓	✓			✓	✓	
3SRIN-X				✓				✓	✓		✓	✓
3SRIN-Y				✓				✓	✓	✓	✓	✓
6SR-X			✓				✓		✓	✓	✓	
6SR-Y			✓				✓		✓	✓	✓	
6SRIN-X				✓			✓		✓			✓
6SRIN-Y				✓			✓		✓	✓	✓	✓

8.2. Variations in Bending Moments in Step-Back Buildings and Regular Buildings with and without Infills

Columns with greater bending moments are more vulnerable during seismic activities. The maximum bending moment of a column can be found for a better understanding of a building's response. As a result, the maximum bending moment of each column was calculated at the third-storey level of the step-back buildings (which is also known as the uphill side of the step-back buildings). The buildings have 16 columns per storey. Due to seismic excitation, the most vulnerable column of the storey was discovered, and that column's maximum bending moment was compared to the three-storey regular and six-storey regular buildings. From Figure 24a, it can be observed that the uphill-side short column is the most affected column. Furthermore, the downhill-side columns in intermediate third and fourth storeys are the most affected, as seen in Figure 24b. Furthermore, the third and fourth storeys from the downhill side again fall in the uphill side of the building. Along the elevation, as shown in Figure 24c, the third storey lies in line with the uphill side of the building. Figure 24c shows the variation in bending moment along the slope for a step-back building, and it can be seen that the short column at the top of the hill attracts larger bending moments than that of the downhill-side-slope column.

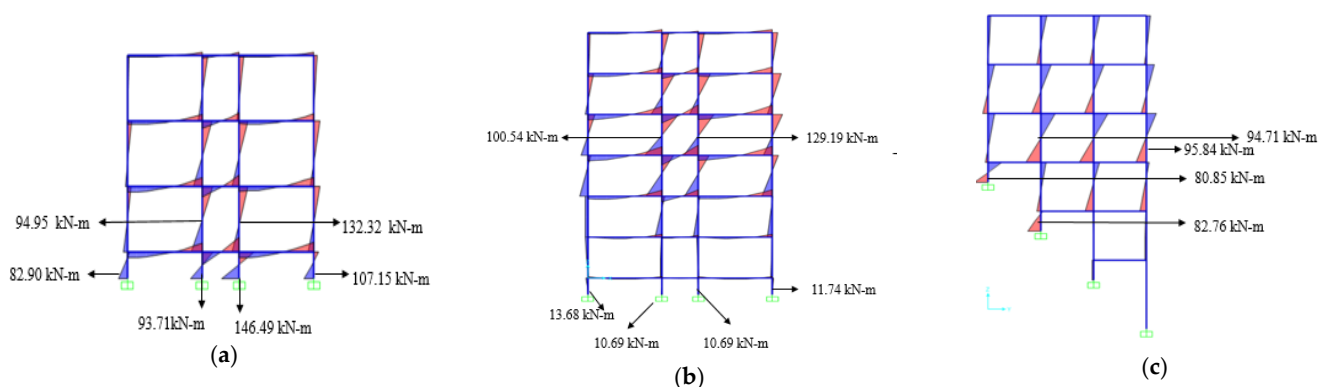


Figure 24. Bending moments of step-back building; (a) uphill side of step-back building; (b) downhill side of step-back building; (c) along the slope.

A similar pattern can be seen in the set-back building with infill walls. From Figure 25a, it can be seen that along the uphill side, the maximum bending moment is in the short column. In contrast, the maximum bending moment in the downhill side is in the column belonging to the fourth storey, which is considered to be a part of the uphill side, as shown in Figure 25b.

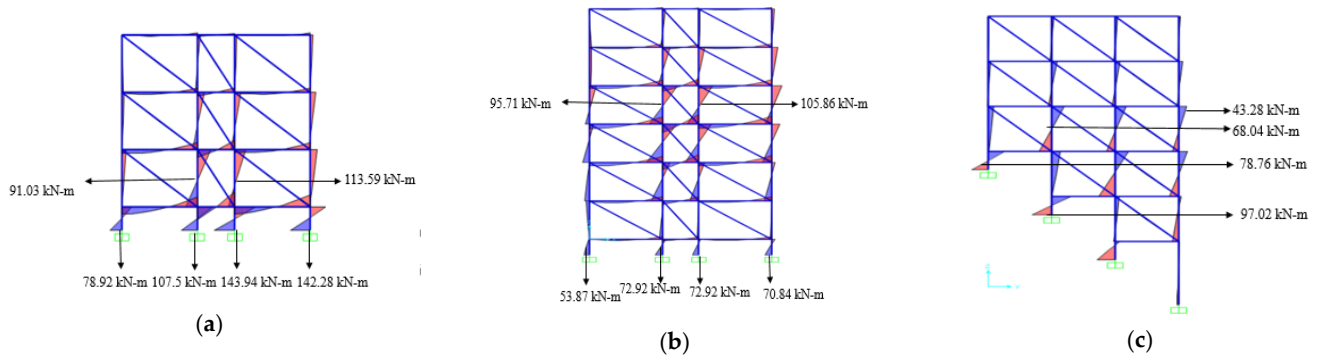


Figure 25. Bending moments of step-back building with infill; (a) uphill side of step-back building; (b) downhill side of step-back building; (c) along the slope.

In a three-storey regular building without infill, the maximum bending moment is in the first-storey intermediate column, as shown in Figure 26a. The maximum bending moment formed in the same building with infill walls is in the short columns, as shown in Figure 26b.

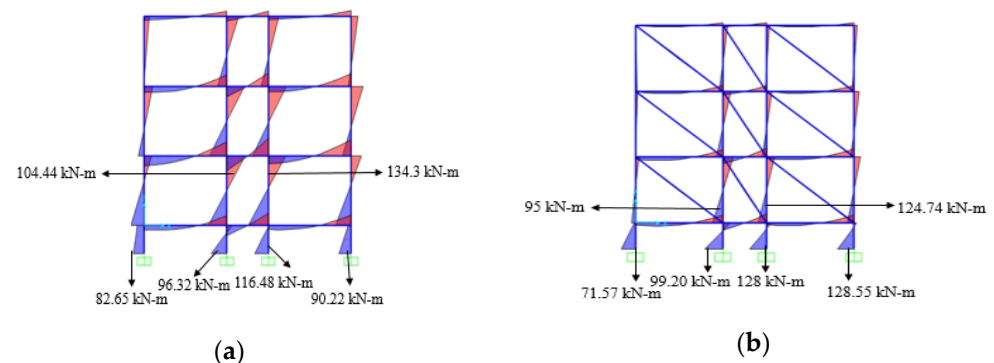


Figure 26. Bending moments of 3-storey regular building (a) without and (b) with infill.

The maximum bending moment in the six-storey regular building with and without infill walls was found to be in the shortest column on the fourth floor of the intermediate columns, as shown in Figure 27a,b.

The study of variation in bending moments for all the study buildings showed that there is a large variation in bending moments in columns along the step-back building when compared with regular buildings. When compared with the three-storey regular building (to represent the uphill side), the bending moment was greater in the step-back building. The downhill side was compared to a six-storey regular building. It was inferred that without infill walls, the maximum bending moment was found in the third and fourth storeys. Analysis of a six-storey regular building showed that the bending moment in the columns gradually decreases with respect to storey height. Further, by incorporating the infill walls in the step-back building, the bending moment was drastically reduced. Hence, the usage of infill walls reduces the bending moment.

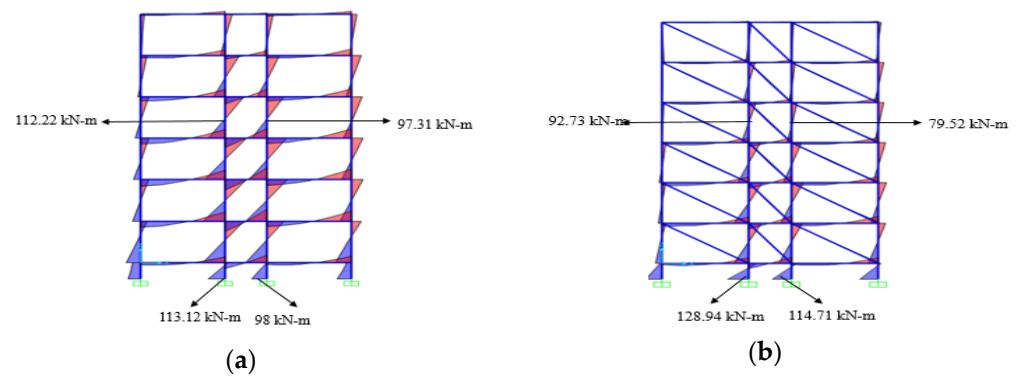


Figure 27. Bending moments of 6-storey regular building (a) without and (b) with infill.

8.3. Results of Non-Linear Time History Analysis

Non-linear time history analysis (NLTHA) was performed on the study buildings for selected ground motions scaled for PGA values of 0.18 g and 0.36 g. The resulting output was plotted in terms of storey displacement and storey drift ratio for each ground motion at each PGA for all study buildings.

8.3.1. Storey Displacement

Seismic evaluation at the global level can be accurately estimated by obtaining storey displacement. In the present study, Figures 28–32 represent the displacements of the uphill sides of the step-back buildings with and without infill walls compared to three-storey regular buildings with and without infill walls for all the considered ground motions. Figures 33–37 represent the displacements of the downhill sides of the step-back buildings with and without infill walls compared to the six-storey regular buildings with and without infill walls for all the considered ground motions. The graphs are plots of storey number vs. storey displacement at PGA levels of 0.18 g and 0.36 g. The dotted line represents the graph for a structure with infill walls, while the straight line indicates the graph for a structure without infill walls. So, for a better understanding of the variations in the results, the means of the ground motions were obtained and plotted in the graphs.

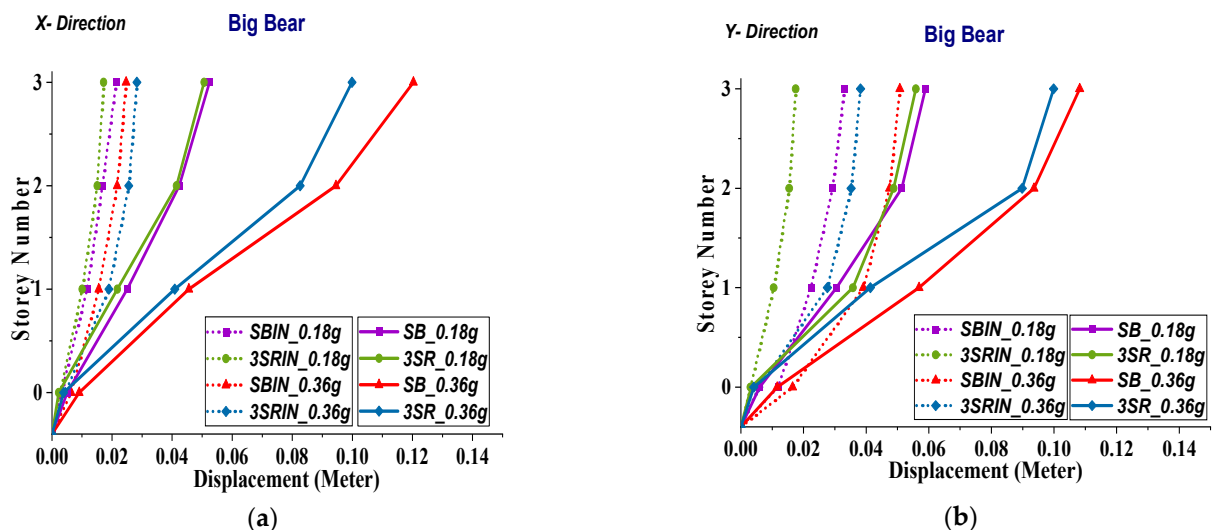


Figure 28. Comparison of storey displacement between the uphill side of step-back building and 3-storey regular building for Big Bear earthquake in (a) X and (b) Y directions.

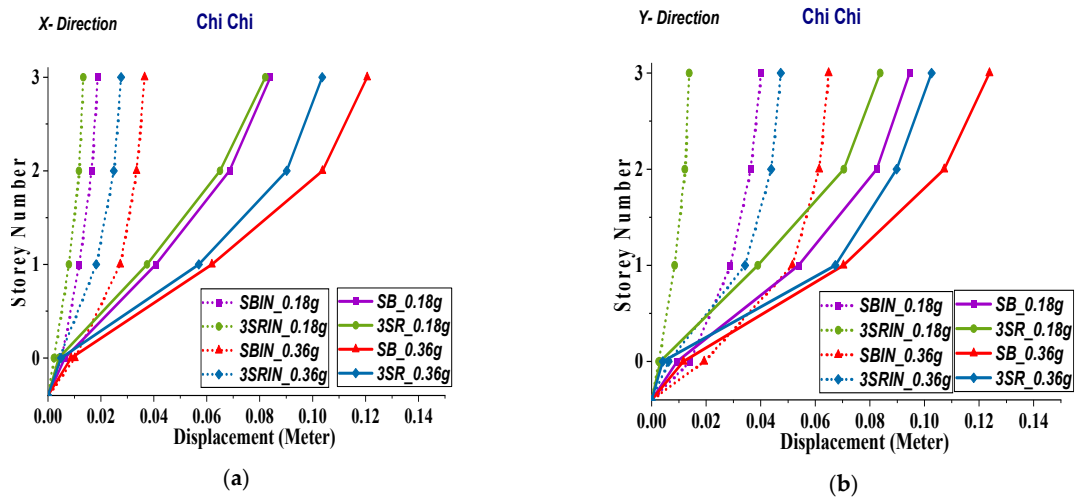


Figure 29. Comparison of storey displacement between the uphill side of step-back building and 3-storey regular building for Chi-Chi earthquake in (a) X and (b) Y directions.

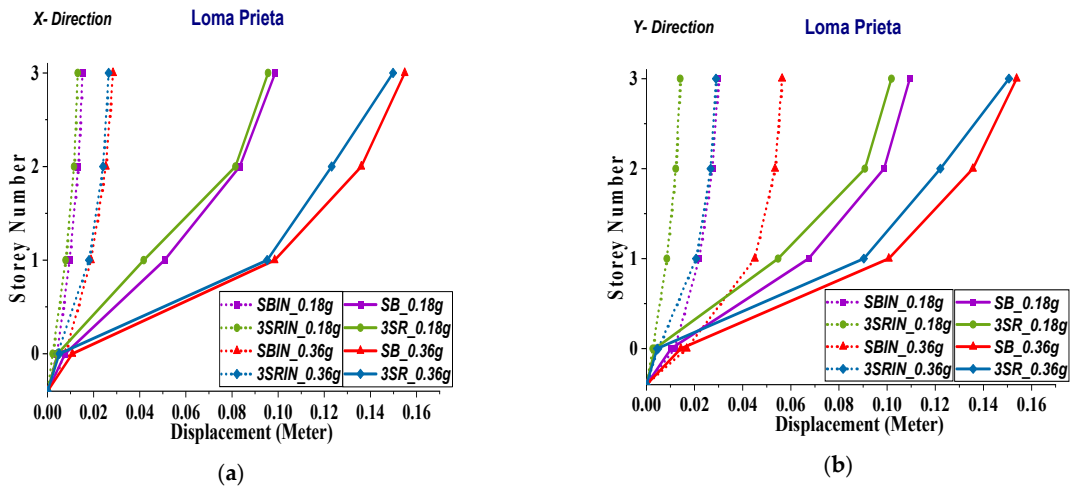


Figure 30. Comparison of storey displacement between the uphill side of step-back building and 3-storey regular building for Loma Prieta earthquake in (a) X and (b) Y directions.

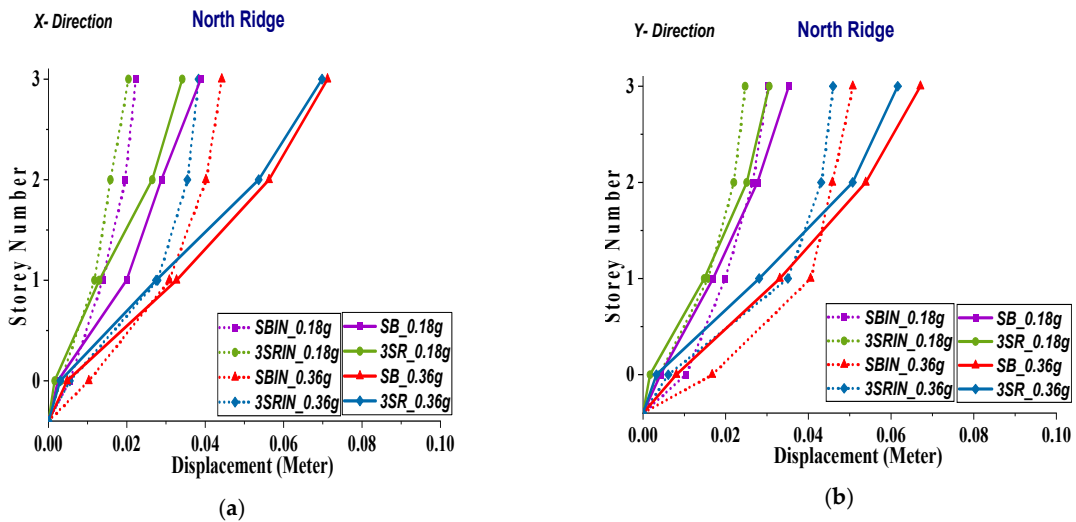


Figure 31. Comparison of storey displacement between the uphill side of step-back building and 3-storey regular building for North Ridge earthquake in (a) X and (b) Y directions.

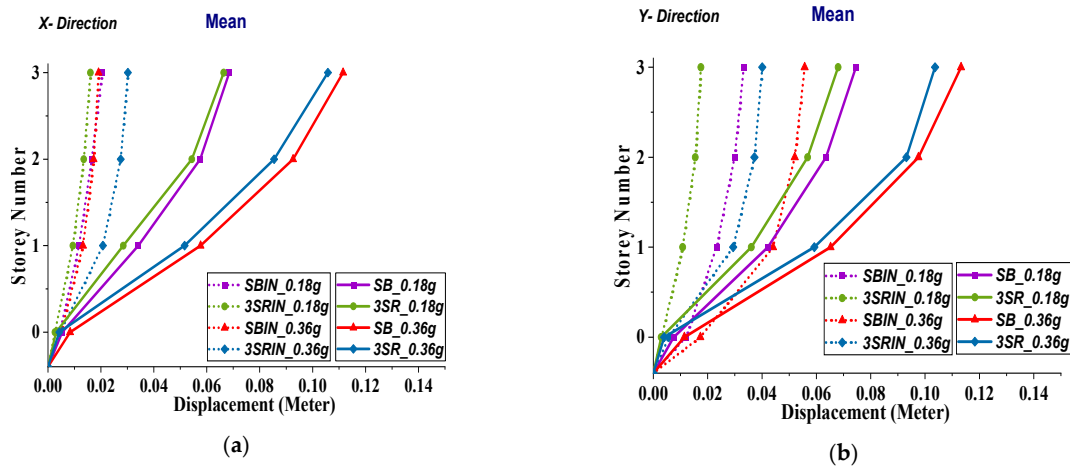


Figure 32. Comparison of storey displacement between the uphill side of step-back building and 3-storey regular building with the help of mean of the earthquakes in (a) X and (b) Y directions.

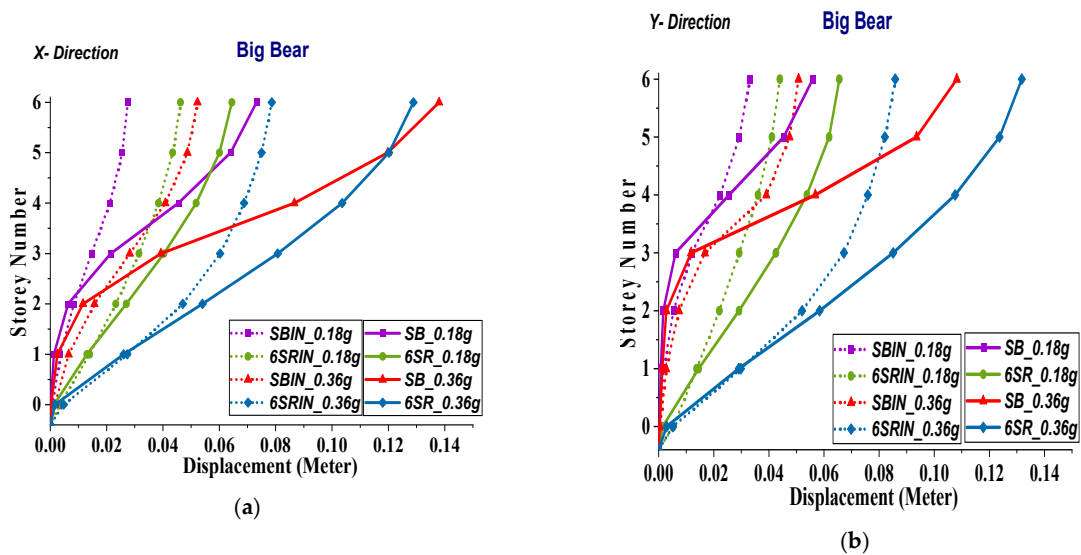


Figure 33. Comparison of storey displacement between the downhill side of step-back building and 6-storey regular building for Big Bear earthquake in (a) X and (b) Y directions.

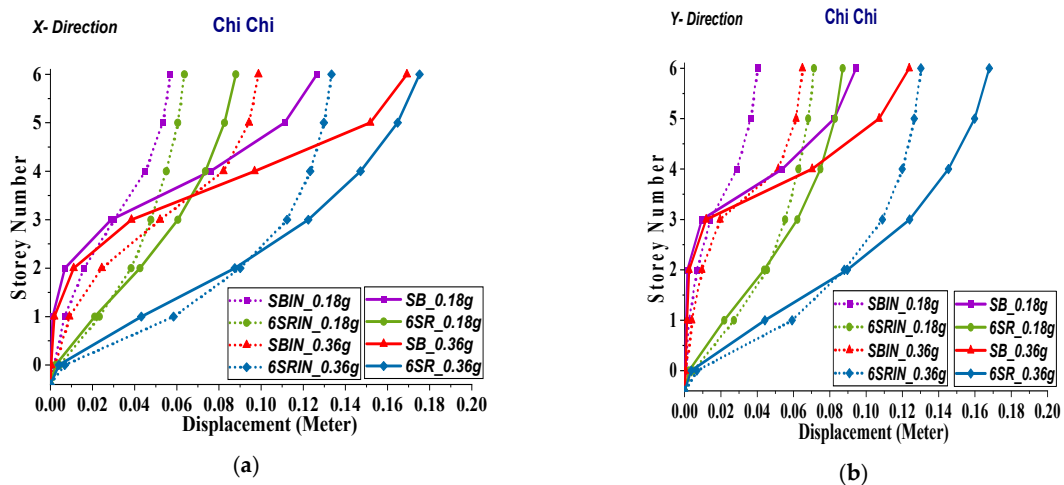


Figure 34. Comparison of storey displacement between the downhill side of step-back building and 6-storey regular building for Chi-Chi earthquake in (a) X and (b) Y directions.

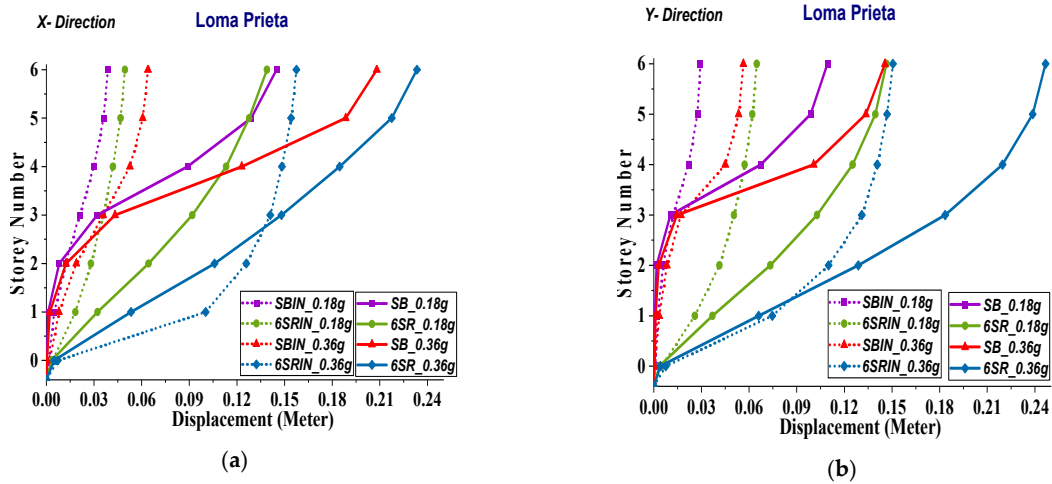


Figure 35. Comparison of storey displacement between the downhill side of step-back building and 6-storey regular building for Loma Prieta earthquake in (a) X and (b) Y directions.

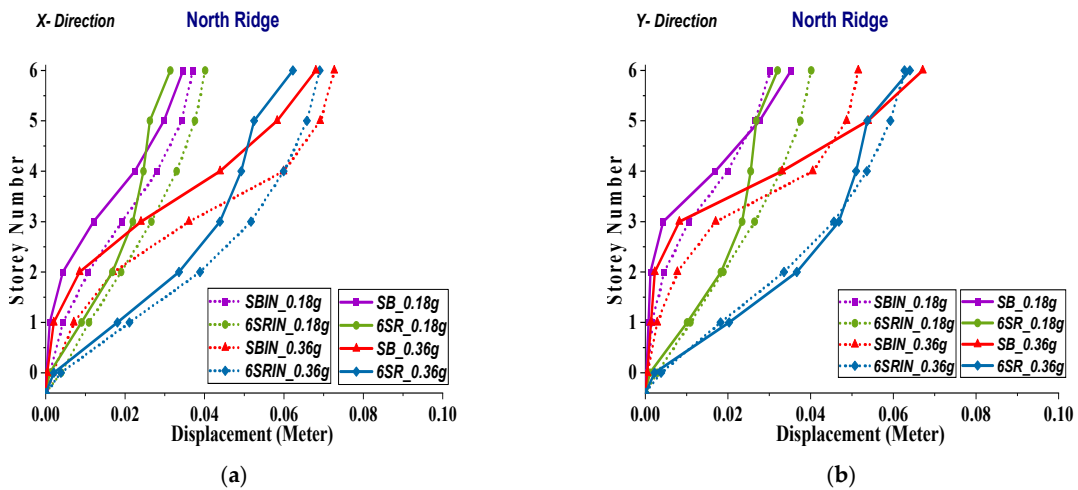


Figure 36. Comparison of storey displacement between the downhill side of step-back building and 6-storey regular building for North Ridge earthquake in (a) X and (b) Y directions.

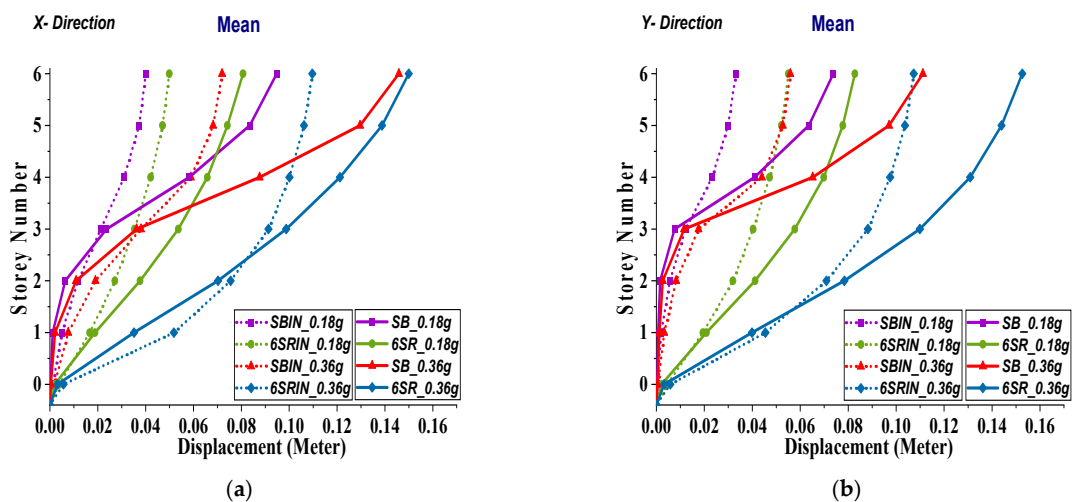


Figure 37. Comparison of storey displacement between the downhill side of step-back building and 6-storey regular building with the mean of the earthquakes in (a) X and (b) Y directions.

The inferences that can be drawn from Figures 28–37, given in Table 10a–d, reveal significant insights into how design features influence building resilience under seismic stress.

Table 10. (a) Comparison of storey displacement of step-back building (uphill side) to the 3-storey regular building, (b) comparison of storey displacement of step-back building with and without infill walls (uphill side), (c) comparison of storey displacement of step-back building (downhill side) to the 6-storey regular building, (d) comparison of storey displacement of step-back building with and without infill walls (downhill side).

(a)				
	X (0.18 g)	Y (0.18 g)	X (0.36 g)	Y (0.36 g)
Big Bear	SB 3.59% greater than 3SR	SB 5.45% greater than 3SR	SB is 4.6% greater than 3SR	SB is 8.34% greater than 3SR
Chi-Chi	SB 5.97% greater than 3SR	SB 11.43% greater than 3SR	SB 14.09% greater than 3SR	SB 17.12% greater than 3SR
Loma Prieta	SB 3.17% greater than 3SR	SB 6.94% greater than 3SR	SB 3.28% greater than 3SR	SB 2.08% greater than 3SR
North Ridge	SB 12.12% greater than 3SR	SB 13.51% greater than 3SR	SB 5.8% greater than 3SR	SB 8.16% greater than 3SR
Mean of above-ground motions	SB 1.68% greater than 3SR	SB 8.8% greater than 3SR	SB 5.14% greater than 3SR	SB 8.43% greater than 3SR
(b)				
	X (0.18 g)	Y (0.18 g)	X (0.36 g)	Y (0.36 g)
Big Bear	SB 51.58% greater than SBIN	SB 44% greater than SBIN	SB 75.38% greater than SBIN	SB 53.08% greater than SBIN
Chi-Chi	SB 76.55% greater than SBIN	SB 57.57% greater than SBIN	SB 69.73% greater than SBIN	SB 47.6% greater than SBIN
Loma Prieta	SB 84.66% greater than SBIN	SB 72.67% greater than SBIN	SB 81.65% greater than SBIN	SB 63.34% greater than SBIN
North Ridge	SB 42.64% greater than SBIN	SB 14.33% greater than SBIN	SB 37% greater than SBIN	SB 24.37% greater than SBIN
Mean of above-ground motions	SB 70% greater than SBIN	SB 55% greater than SBIN	SB 83% greater than SBIN	SB 51% greater than SBIN
(c)				
	X (0.18g)	Y (0.18g)	X (0.36g)	Y (0.36g)
Big Bear	SB 12% greater than 6SR	6SR 14.74% greater than SB	SB 6.59% greater than 6SR	6SR 18% greater than SB
Chi-Chi	SB 30.41% greater than 6SR	SB 7.86% greater than 6SR	6SR 3.42% greater than SB	6SR 26.26% greater than SB
Loma Prieta	SB 4.14% greater than 6SR	6SR 25.32% greater than SB	6SR 10.83% greater than SB	6SR 40.98% greater than SB
North Ridge	SB 9.32% greater than 6SR	Step-back 9.32% greater than 6SR	SB 8.48% greater than 6SR	SB 4.63% greater than 6SR
Mean of above-ground motions	SB 15% greater than 6SR	6SR 11% greater than SB	6SR 3% greater than SB	6SR 27% greater than SB

Table 10. Cont.

(d)				
	X (0.18 g)	Y (0.18 g)	X (0.36 g)	Y (0.36 g)
Big Bear	SB 62.39% greater than SBIN	SB 40.98% greater than SBIN	SB 62.13% greater than SBIN	SB 53.04% greater than SBIN
Chi-Chi	SB 55.01% greater than SBIN	SB 57.56% greater than SBIN	SB 41.63% greater than SBIN	SB 47.57% greater than SBIN
Loma Prieta	SB 74.44% greater than SBIN	SB 73.21% greater than SBIN	SB 69.23% greater than SBIN	SB 61.27% greater than SBIN
North Ridge	SBIN 6.48% greater than SB	SB 14.33% greater than SBIN	SBIN 6.39% greater than SB	SB 23.23% greater than SBIN
Mean of above-ground motions	SB 58% greater than SBIN	SB 55% greater than SBIN	SB 51% greater than SBIN	SB 50% greater than SBIN

From Table 10a, it can be observed that a step-back building (SB) generally exhibits greater displacement compared to a regular three-storey building (3SR), especially at higher seismic accelerations (0.36 g), where the mean displacement in an SB is 5.14% greater in the X direction and 8.43% greater in the Y direction than in a 3SR. This indicates the increased sensitivity of SB designs to seismic forces, emphasizing the need for specialized structural considerations for such buildings.

In Table 10b, the comparison of SBs with (SBIN) and without (SB) infill walls under seismic conditions shows that infill walls markedly reduce seismic-induced displacements in SBs. At a seismic acceleration of 0.36 g, the mean displacement of an SB is 83% greater in the X direction and 51% greater in the Y direction than an SBIN, highlighting the critical role of infill walls in enhancing earthquake resilience. Table 10c compares the displacement of an SB (downhill side) with a six-storey regular building (6SR). The data indicate a directionally dependent structural response: at 0.36 g, the 6SR shows a mean displacement 3% greater in the X direction and 27% greater in the Y direction than the SB, suggesting different seismic reinforcement strategies for various building configurations. Lastly, Table 10d shows an analysis of the impact of infill walls on SBs (downhill side). At 0.36 g seismic acceleration, the SB displays a mean displacement 51% greater in the X direction and 50% greater in the Y direction than the SBIN, reinforcing the importance of infill walls in mitigating seismic impacts, particularly in earthquake-prone areas. In summary, these tables collectively underscore the nuanced effects of building design elements like step-back features and infill walls on seismic performance, highlighting their significance in building design for earthquake resilience.

8.3.2. Inter-Storey Drift Ratio

The storey drift ratio is the relative translational displacement between two consecutive floors divided by the storey height. It is a critical engineering response quantity and structural performance indicator. Several aspects of structural engineering would benefit greatly from accurate storey drift ratio measurements, particularly for structures subjected to inelastic deformations [41]. The storey drift ratios of step-back, three-storey regular, and six-storey regular buildings with and without infills are illustrated in Figures 38–47. The storey drift ratio graphs are drawn in the same manner as the storey displacement graphs, at PGAs of 0.18 g and 0.36 g. Figures 38–42 represent the storey drift ratio of the uphill side of step-back buildings with and without infill walls to three-storey regular buildings with and without infill walls for all the considered ground motions. Figures 43–47 represent the storey drift ratios of the downhill sides of the step-back buildings with and without infill walls to the six-storey regular buildings with and without infill walls for all the considered ground motions. The graphs are plots of storey number vs. storey drift ratio at PGA levels of 0.18 g and 0.36 g. The dotted line represents the graph for a structure with infill walls,

while the straight line indicates the graph for a structure without infill walls. So, for a better understanding of the variations in results, the mean of the earthquakes graph is plotted.

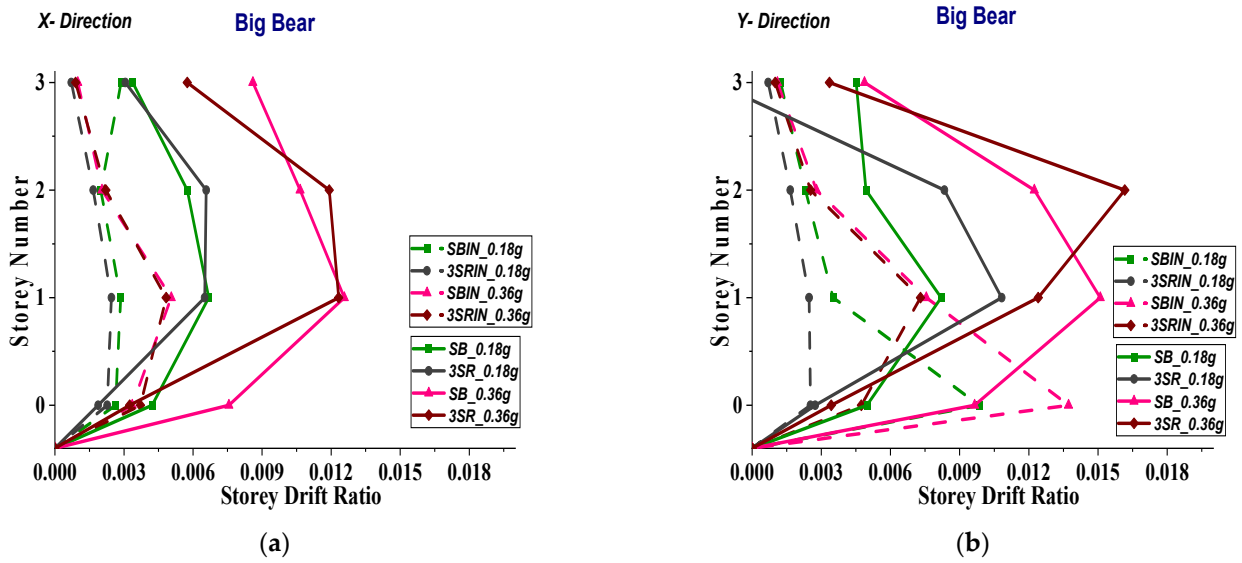


Figure 38. Comparison of storey drift ratio between the uphill side of step-back building and 3-storey regular building for Big Bear ground motion in (a) X and (b) Y directions.

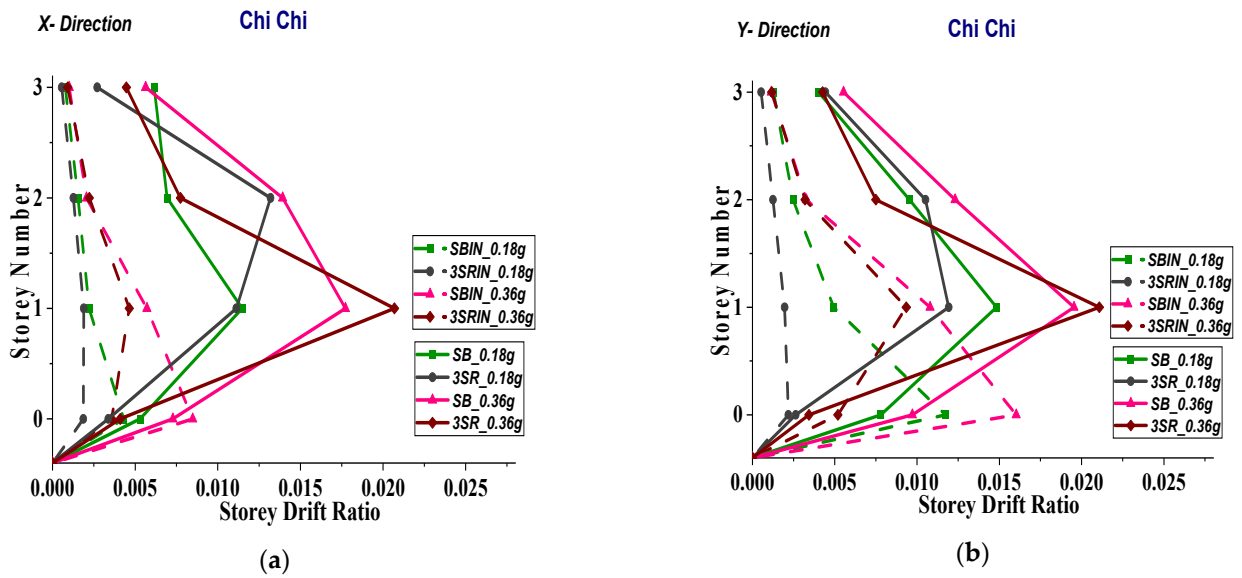


Figure 39. Comparison of storey drift ratio between the uphill side of the step-back building and 3-storey regular building for Chi-Chi ground motion in (a) X and (b) Y directions.

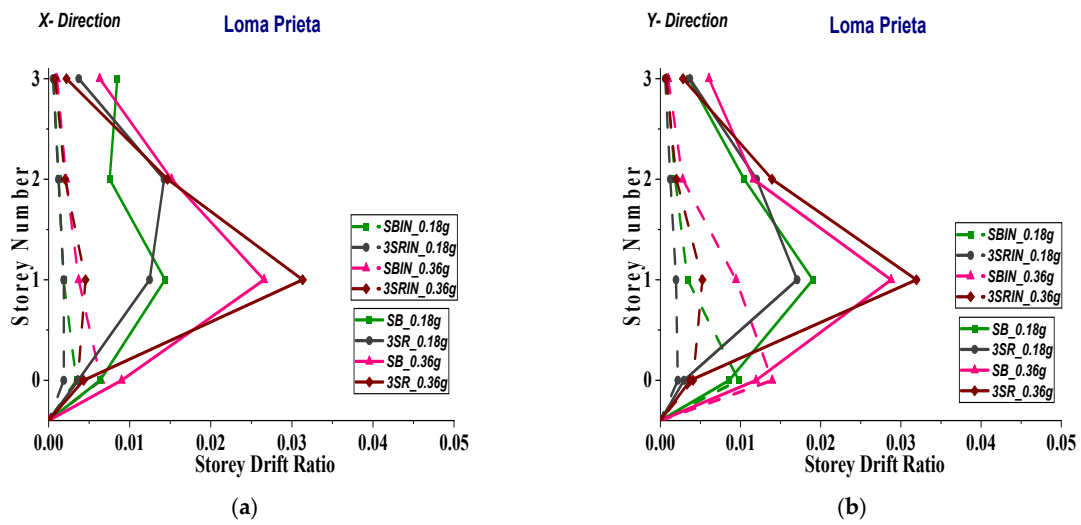


Figure 40. Comparison of storey drift ratio between the uphill side of step-back building and 3-storey regular building for Loma Prieta ground motion in (a) X and (b) Y directions.

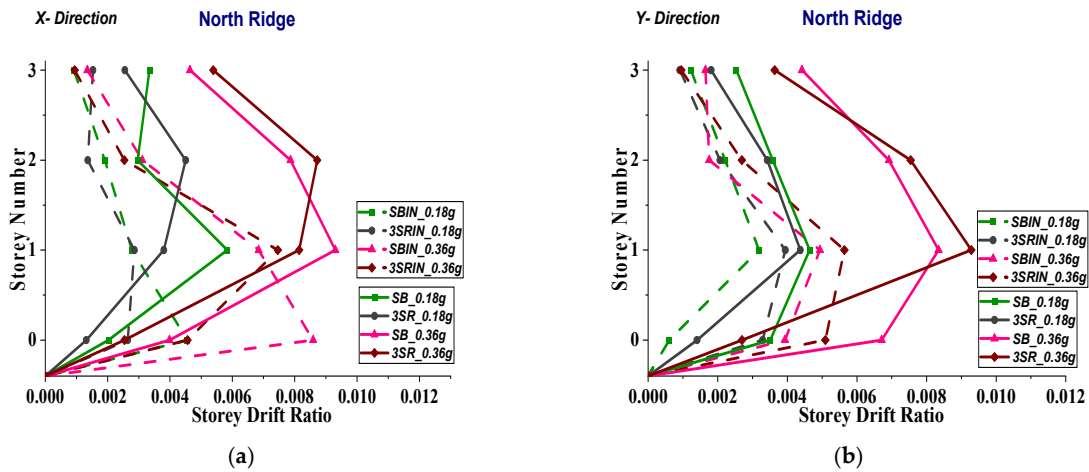


Figure 41. Comparison of storey drift ratio between the uphill side of step-back building and 3-storey regular building for North Ridge ground motion in (a) X and (b) Y directions.

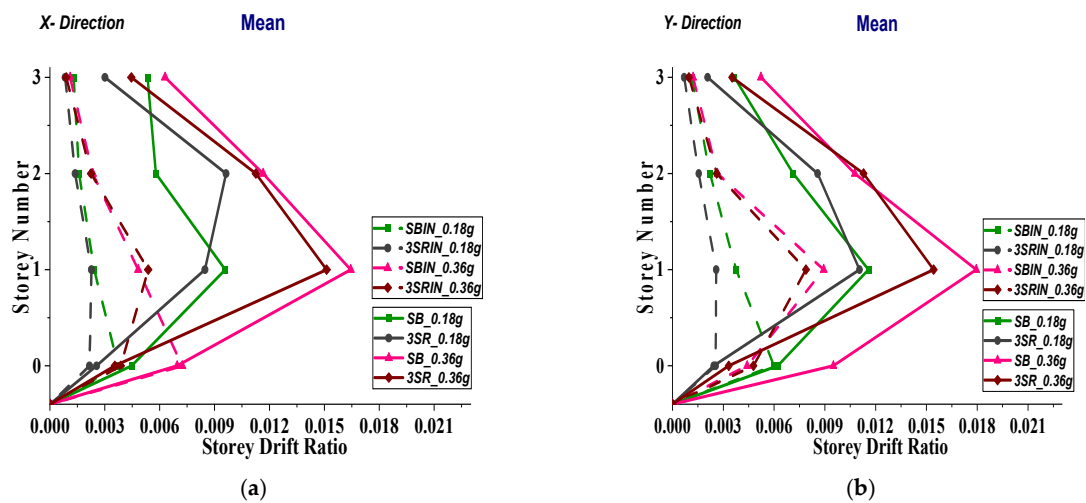


Figure 42. Comparison of storey drift ratio between the uphill side of step-back building and 3-storey regular building with the mean of the ground motions in (a) X and (b) Y directions.

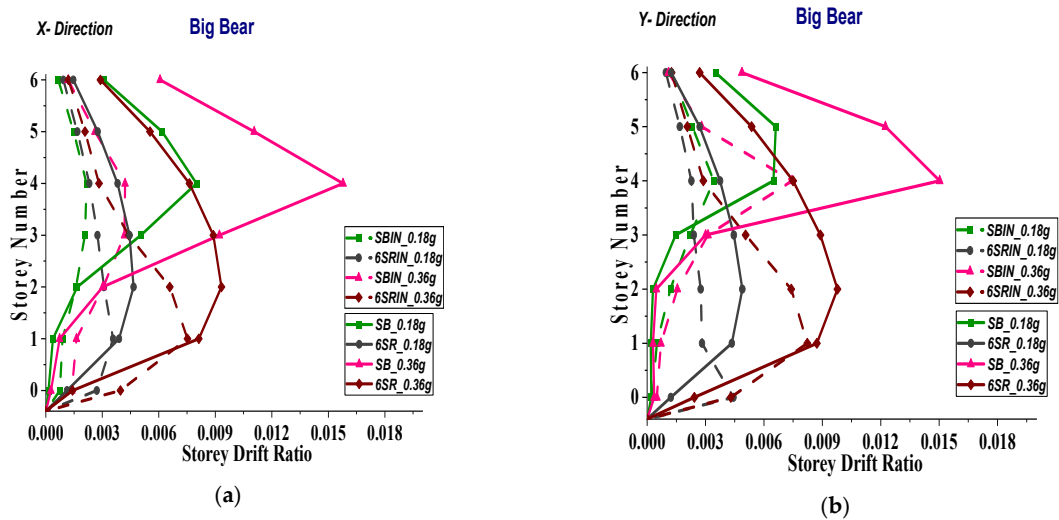


Figure 43. Comparison of storey drift ratio between the downhill side of step-back building and 6-storey regular building for Big Bear ground motion in (a) X and (b) Y directions.

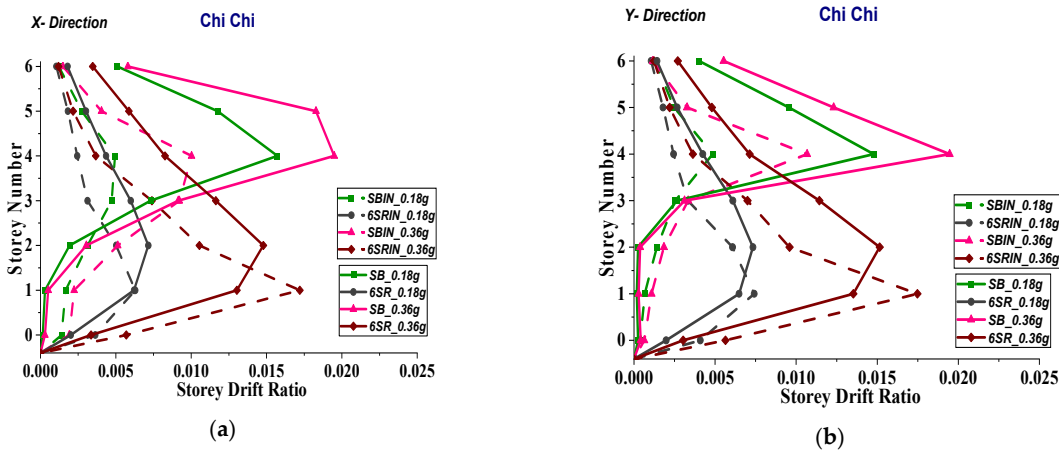


Figure 44. Comparison of storey drift ratio between the downhill side of step-back building and 6-storey regular building for Chi-Chi ground motion in (a) X and (b) Y directions.

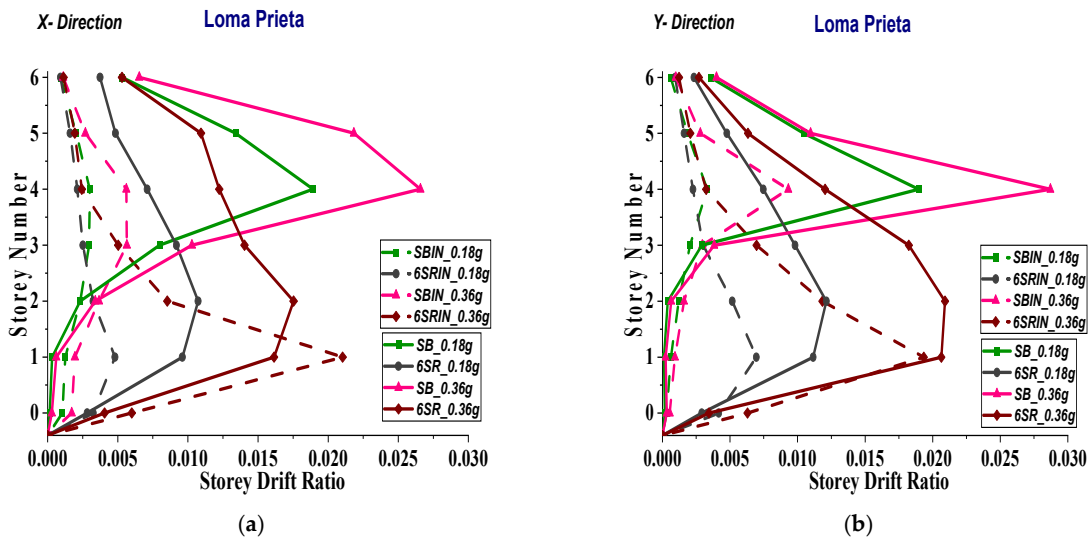


Figure 45. Comparison of storey drift ratio between the downhill side of step-back building and 6-storey regular building for Loma Prieta ground motion in (a) X and (b) Y directions.

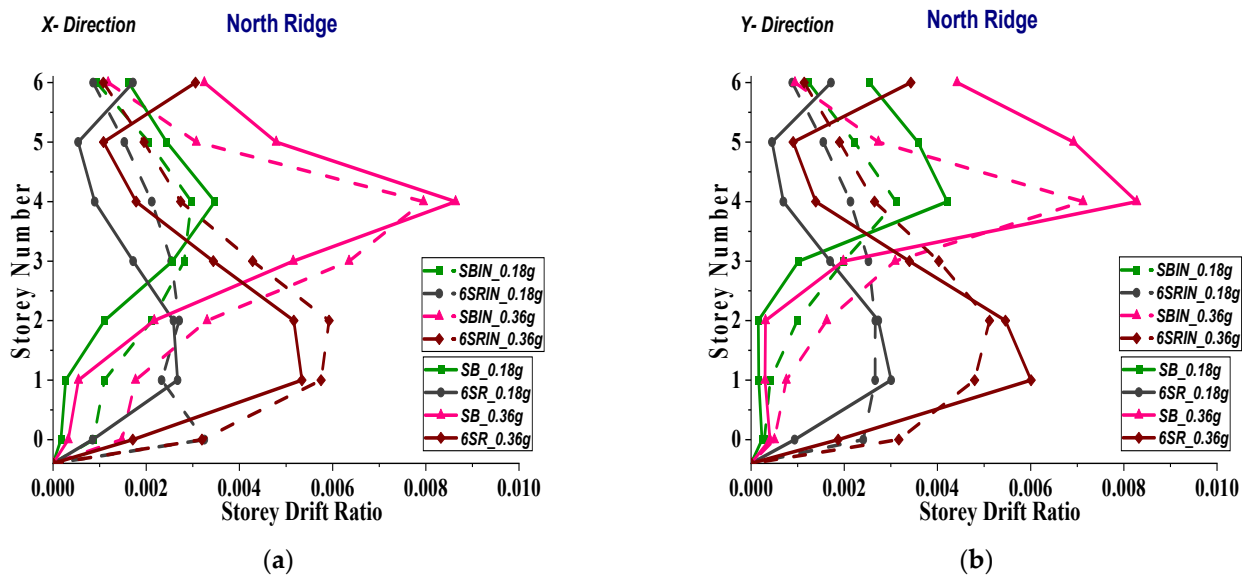


Figure 46. Comparison of storey drift ratio between the downhill side of step-back building and 6-storey regular building for North Ridge ground motion in (a) X and (b) Y directions.

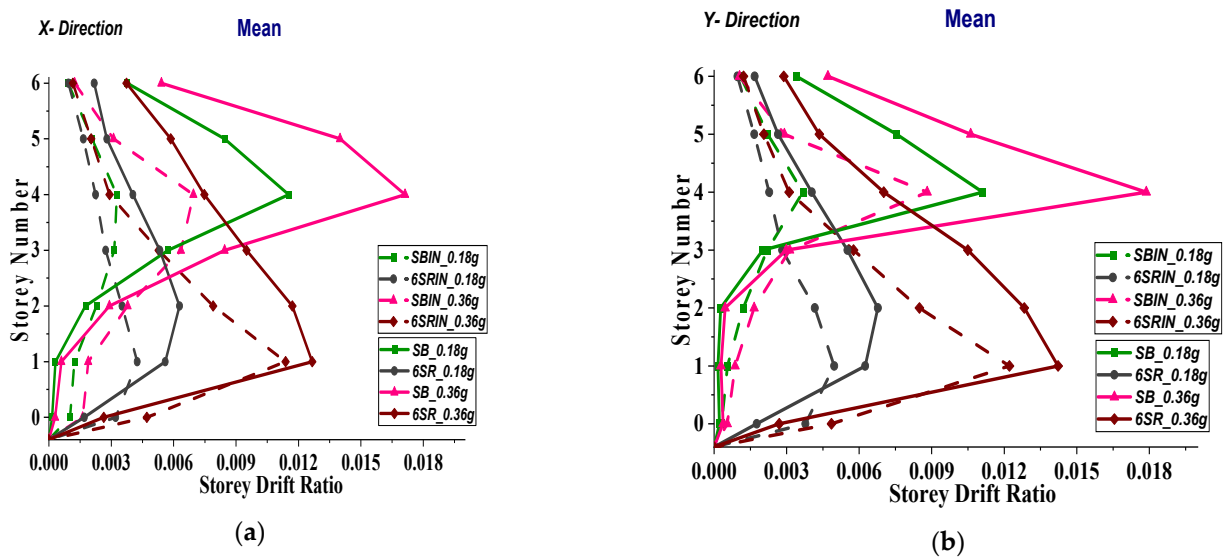


Figure 47. Comparison of storey drift ratio between the downhill side of step-back building and 6-storey regular building with the mean of the ground motions in (a) X and (b) Y directions.

From Table 11a–d, the seismic performance of step-back buildings (SBs) is examined in terms of storey drift ratios under various conditions. Table 11a indicates that the SB on the uphill side shows a mean drift ratio 15.11% greater in the X direction and 4.57% greater in the Y direction compared to a three-storey regular building (3SR). Table 11b demonstrates the effectiveness of infill walls (SBIN), where the SB without infill walls exhibits mean drift ratios 74.75% and 33% higher in the X and Y directions, respectively. In Table 11c, when comparing the SB on the downhill side to a six-storey regular building (6SR), the mean drift ratio of the SB is significantly higher, at 79.17% in the X direction and 63.66% in the Y direction. Finally, Table 11d further emphasizes the role of infill walls; the SB without them on the downhill side shows a mean drift ratio increase of 71.64% in the X direction and 30.28% in the Y direction. These findings highlight the substantial impact of building design elements like infill walls and orientation (uphill or downhill) on the seismic drift ratios, indicating their critical importance in designing earthquake-resistant structures.

Table 11. (a) Comparison of storey drift ratios of step-back buildings (uphill side) to 3-storey regular buildings, (b) comparison of storey drift ratios of step-back buildings with and without infill walls (uphill side), (c) comparison of storey drift ratios of step-back buildings (downhill side) to 6-storey regular buildings, (d) comparison of storey drift ratios of step-back buildings with and without infill walls (downhill side).

(a)				
	X (0.18 g)	Y (0.18 g)	X (0.36 g)	Y (0.36 g)
Big Bear	SB 2.58% greater than 3SR	3SR 24.25% greater than SB	SB 2.28% greater than 3SR	SB 17.84% greater than 3SR
Chi-Chi	SB 3.01% greater than 3SR	SB 19.63% greater than 3SR	3SR 12.33% greater than SB	3SR 24% greater than SB
Loma Prieta	SB 13.25% greater than 3SR	SB 10.32% greater than 3SR	3SR 14.22% greater than SB	3SR 8.86% greater than SB
North Ridge	SB 34.92% greater than 3SR	3SR 3% greater than SB	SB 12.46% greater than 3SR	3SR 1.73% greater than SB
Mean	SB 15.11% greater than 3SR	SB 4.57% greater than 3SR	SB 9.29% greater than 3SR	SB 3.61% greater than 3SR
(b)				
	X (0.18 g)	Y (0.18 g)	X (0.36 g)	Y (0.36 g)
Big Bear	SB 57.22% greater than SBIN	SB 57.22% greater than SBIN	SB 74.9% greater than SBIN	SB 49.97% greater than SBIN
Chi-Chi	SB 80.73% greater than SBIN	SB 66.72% greater than SBIN	SB 67.80% greater than SBIN	SB 11.97% greater than SBIN
Loma Prieta	SB 87.22% greater than SBIN	SB 82.12% greater than SBIN	SB 86.08% greater than SBIN	SB 67.22% greater than SBIN
North Ridge	SB 52.4% greater than SBIN	SB 24.88% greater than SBIN	SB 70.65% greater than SBIN	SB 4.89% greater than SBIN
Mean	SB 74.75% greater than SBIN	SB 33% greater than SBIN	SB 70.65% greater than SBIN	SB 50.23% greater than SBIN
(c)				
	X (0.18 g)	Y (0.18 g)	X (0.36 g)	Y (0.36 g)
Big Bear	SB 52.35% greater than 6SR	SB 42.22% greater than 6SR	SB 51.7% greater than 6SR	SB 50.13% greater than 6SR
Chi-Chi	SB 72.30% greater than 6SR	SB 71.29% greater than 6SR	SB 57.59% greater than 6SR	SB 63.36% greater than 6SR
Loma Prieta	SB 62.51% greater than 6SR	SB 60.63% greater than 6SR	SB 53.97% greater than 6SR	SB 57.90% greater than 6SR
North Ridge	SB 74.28% greater than 6SR	SB 83.53% greater than 6SR	SB 73.14% greater than 6SR	SB 83.25% greater than 6SR
Mean	SB 79.17% greater than 6SR	SB 63.66% greater than 6SR	SB 56.33% greater than 6SR	SB 60.76% greater than 6SR
(d)				
	X (0.18 g)	Y (0.18 g)	X (0.36 g)	Y (0.36 g)
Big Bear	SB 72.96% greater than SBIN	SB 47.16% greater than SBIN	SB 73.32% greater than SBIN	SB 50.48% greater than SBIN
Chi-Chi	SB 68.04% greater than SBIN	SB 67.18% greater than SBIN	SB 48.54% greater than SBIN	SB 45.17% greater than SBIN

Table 11. Cont.

(d)				
	X (0.18 g)	Y (0.18 g)	X (0.36 g)	Y (0.36 g)
Loma Prieta	SB 84.14% greater than SBIN	SB 82.56% greater than SBIN	SB 78.89% greater than SBIN	SB 67.56% greater than SBIN
North Ridge	SB 14.49% greater than SBIN	SB 26.12% greater than SBIN	SB 16.47% greater than SBIN	SB 15.5% greater than SBIN
Mean	SB 71.64% greater than SBIN	SB 30.28% greater than SBIN	SB 59.41% greater than SBIN	SB 50.69% greater than SBIN

9. Conclusions

The seismic vulnerability assessment of RC structures was analysed in accordance with the IS code, and three-dimensional analytical models of the buildings have been built and investigated using non-linear static pushover analysis and dynamic analysis. The following conclusions are formed based on the outcomes of non-linear analyses:

- Capacity curves show that step-back buildings with infill are significantly stronger and stiffer compared to those without infill, a trend also seen in both three- and six-storey regular buildings.
- At the DBE performance point, short columns in step-back buildings exhibit considerable damage, whereas intermediate columns in regular buildings show less damage. However, at the MCE performance point, severe damage is observed in both step-back building types, regardless of infill presence.
- The uphill side of step-back buildings experiences greater bending moments than three-storey regular buildings due to higher slopes and short columns. Step-back buildings without infill have higher bending moments compared to those with infill, as infill adds stiffness. However, the bending moments on the downhill side of step-back and six-storey regular buildings were less clear due to their configuration.
- Time history analysis reveals that the uphill displacement in step-back buildings is greater than in three-storey regular buildings, but less from the downhill side compared to six-storey regular buildings. Step-back buildings without infill show greater displacement than those with infill, highlighting the stiffness added by infill walls.
- Storey drift ratio analysis indicates that step-back buildings without infill have higher drift ratios than those with infill. The first storey on the uphill side and the fourth storey on the downhill side of step-back buildings are particularly vulnerable to seismic activity, suggesting severe damage on the uphill side.
- The results, while informative, are based on several assumptions and idealizations, such as neglecting foundation and soil–structure interaction effects. Further refined studies, incorporating non-linear dynamic analysis with real ground motion data and considering foundation modelling with soil–structure interaction, are necessary for more accurate assessments.

Author Contributions: Conceptualization, B.R. and V.R.; Data curation, B.R.; Formal analysis, V.R.; Funding acquisition, A.A. and M.F.S.; Investigation, B.B.B. and A.I.S.; Methodology, B.R. and V.R.; Project administration, A.A. and A.I.S.; Resources, M.F.S. and A.A.; Software, B.R. and V.R.; Supervision, A.I.S.; Validation, B.B.B. and R.V.; Visualization, M.F.S. and R.V.; Writing—original draft, B.R. and V.R.; Writing—review and editing, A.I.S. All authors have read and agreed to the published version of the manuscript.

Funding: This research was conducted without external funding support.

Data Availability Statement: The data presented in this study are available on request from the corresponding author. The data are not publicly available due to our research is currently ongoing.

Conflicts of Interest: The authors declare no conflict of interest.

Abbreviations

ASCE	American Society of Civil Engineering
ATC	Applied Technology Council
CP	Collapse prevention
DBE	Design Basis Earthquake
FEMA	Federal Emergency Management Agency
IO	Immediate occupancy
IN	Infill
IC	Intermediate column
IS	Indian Standard
LS	Life safety
MCE	Maximum Considered Earthquake
Mw	Moment magnitude
NLTHA	Non-linear time history analysis
OC	Outer column
PGA	Peak ground acceleration
PP	Performance point
RC	Reinforced concrete
SAP	Structural analysis program
SB	Step-back building
SBIN	Step-back building with infill
SC	Short column
S.F.	Scale factor
URM	Un-reinforced masonry
3D	Three-dimensional
3SR	Three-storey regular building
3SRIN	Three-storey regular building with infill
6SR	Six-storey regular building
6SRIN	Six-storey regular building with infill

Notation

a	Width of the diagonal strut
b	Width
d	Depth
d_b	Diameter of the longitudinal reinforcement
E_m	Modulus of elasticity of masonry prism
E_{me}	Excepted modulus of elasticity of infill material
E_{fe}	Excepted modulus of elasticity of frame
f_b	Compressive strength of brick
f_m	Compressive strength of masonry prism
f_{mo}	Compressive strength of mortar
f_y	Yield strength of longitudinal steel
h_{col}	Column height between centre lines of beams
h_{inf}	Height of infill panel
I_{col}	Moment of inertia of column
L	Length
L_{inf}	Length of infill panel
l_p	Plastic hinge length
r_{inf}	Diagonal length of the infill panel
t_{inf}	Thickness of infill panel
λ_1	Coefficient to determine the equivalent width of the infill strut

References

1. Halder, L.; Chandra Dutta, S.; Sharma, R.P.; Bhattacharya, S. Lessons Learnt from Post-Earthquake Damage Study of Northeast India and Nepal during Last Ten Years: 2021 Assam Earthquake, 2020 Mizoram Earthquake, 2017 Ambasa Earthquake, 2016 Manipur Earthquake, 2015 Nepal Earthquake, and 2011 Sikkim Earthquake. *Soil Dyn. Earthq. Eng.* **2021**, *151*, 106990. [CrossRef]
2. Surana, M.; Singh, Y.; Lang, D.H. Fragility Analysis of Hillside Buildings Designed for Modern Seismic Design Codes. *Struct. Des. Tall Spec. Build.* **2018**, *27*, e1500. [CrossRef]
3. Surana, M.; Meslem, A.; Singh, Y.; Lang, D.H. Analytical Evaluation of Damage Probability Matrices for Hill-Side RC Buildings Using Different Seismic Intensity Measures. *Eng. Struct.* **2020**, *207*, 110254. [CrossRef]
4. Singh, Y.; Yeluguri, V.R.; Lang, D.H. Seismic response of hill buildings subjected to bi-directional excitation. In Proceedings of the 10th US National Conference on Earthquake Engineering, Anchorage, Alaska, 21–25 July 2014.
5. Dizhur, D.; Dhakal, R.P.; Bothara, J.; Ingham, J.M. Building Typologies and Failure Modes Observed in the 2015 Gorkha (Nepal) Earthquake. *Bull. N. Z. Soc. Earthq. Eng.* **2016**, *49*, 211–232. [CrossRef]
6. Singh, Y.; Gade, P.; Lang, D.; Erduran, E. Seismic Behavior of Buildings Located on Slopes—An Analytical Study and Some Observations from Sikkim Earthquake of 18 September 2011. Available online: https://www.iitk.ac.in/nicee/wcee/article/WCEE2012_4201.pdf (accessed on 8 April 2020).
7. Kumar, S. A simplified method for elastic seismic analysis of hill buildings. *J. Earthq. Eng.* **1998**, *2*, 241. [CrossRef]
8. CSI. *SAP2000 V. 8, 2002. Integrated Finite Element Analysis and Design of Structures Basic Analysis Reference Manual*; Computers and Structures, Inc.: Berkeley, CA, USA, 2010.
9. Birajdar, B.; Nalawade, S. Seismic Analysis of Buildings Resting on Sloping Ground. Available online: https://www.iitk.ac.in/nicee/wcee/article/13_1472.pdf (accessed on 1 January 2004).
10. Available online: <https://www.mapsofindia.com> (accessed on 1 January 2022).
11. Liu, L.; Li, Y.; Zheng, N.; Xie, Q. Seismic Response of Stepped Building Supported by Stepped Foundation on Hillside, Cunxiong Wu; 2017. Available online: <https://www.wcee.nicee.org/wcee/article/16WCEE/WCEE2017-2150.pdf> (accessed on 12 December 2023).
12. Kumar, A. Impact of Building Regulations on Indian Hill Towns. *HBRC J.* **2016**, *12*, 316–326. [CrossRef]
13. Surana, M.; Singh, Y.; Lang, D.H. Seismic Characterization and Vulnerability of Building Stock in Hilly Regions. *Nat. Hazards Rev.* **2018**, *19*, 04017024. [CrossRef]
14. Raj, D.; Singh, Y.; Kaynia, A.M. Seismic Fragility Analysis of Coupled Building-Slope Systems. *Earthq. Eng. Struct. Dyn.* **2023**, *53*, 116–137. [CrossRef]
15. Farghaly, A.A. Evaluation of seismic performance of buildings constructed on hillside slope of Doronka village-Egypt. *Int. Sch. Res. Not.* **2014**, *2014*, 1–13. [CrossRef]
16. Welsh-Huggins, S.J. Seismic Vulnerability of Hillside Buildings in Northeast India. Ph.D. Thesis, University of Colorado at Boulder, Boulder, CO, USA, 2016.
17. Surana, M.; Singh, Y.; Lang, D.H. Effect of Irregular Structural Configuration on Floor Acceleration Demand in Hill-Side Buildings. *Earthq. Eng. Struct. Dyn.* **2018**, *47*, 2032–2054. [CrossRef]
18. Kumar, A. Review of Building Regulations for Safety against Hazards in Indian Hill Towns. *J. Urban Manag.* **2018**, *7*, 97–110. [CrossRef]
19. Murty, C.V.R.; Raghukanth, S.T.G.; Menon, A.; Goswami, R.; Vijayanarayanan, A.R.; Gandhi, S.R.; Satyanarayana, K.N. The Mw 6.9 Sikkim-Nepal Border Earthquake of 18 September 2011. In *EERI Newsletter, EERI Special Earthquake Report*; Earthquake Engineering Research Institute: Oakland, CA, USA, 2012; pp. 1–14.
20. *IS-1893-2016 (Part-1)*; Criteria for Earthquake Resistant Design of Structure. Bureau of Indian Standards: New Delh, India, 2016.
21. Gupta, S.; Chandra, P.G. A review on short column seismic Behavior and Their prevention on sloping ground. *J. Civ. Eng. Environ. Technol.* **2016**, *3*, 6.
22. Murty, C.V.R. *Why Are Short Columns More Damaged during Earthquakes?* Indian Institute of Technology Kanpur: Kanpur, India, 2004.
23. Işık, E.; Ulutaş, H.; Harirchian, E.; Avcil, F.; Aksoylu, C.; Arslan, M.H. Performance-Based Assessment of RC Building with Short Columns due to the Different Design Principles. *Buildings* **2023**, *13*, 750. [CrossRef]
24. Jarapala, R.; Menon, A. Seismic Performance of Reinforced Concrete Buildings on Hill Slopes: A Review. *J. Inst. Eng. (India) Ser. A* **2023**, *104*, 721–745. [CrossRef]
25. *IS-13920-1993*; Practice for Ductile Detailing of Reinforced Concrete Structures. Bureau of Indian Standards: New Delh, India, 1993.
26. Mohammad, Z. Effect of Un-reinforced Masonry Infills on Seismic Performance of Hill Buildings. *VW Appl. Sci.* **2019**, *1*, 37–47. [CrossRef]
27. Kaushik, H.B.; Durgesh, C.R.; Sudhir, K.J. Stress-strain characteristics of clay brick masonry under uniaxial comparison. *J. Mater. Civ. Eng.* **2007**, *19*, 728–739. [CrossRef]
28. Usta, P.; Özge, O.; Özgür, B. Effect of masonry infill walls on the nonlinear response of reinforced concrete structure: October 30, 2020 İzmir earthquake case. *Eng. Fail. Anal.* **2023**, *146*, 107081. [CrossRef]
29. Guettala, S.; Abdesselam, I.; Chebili, R.; Guettala, S. Assessment of the Effects of Infill Walls' Layout in Plan and/or Elevation on the Seismic Performance of 3D Reinforced Concrete Structures. *Asian J. Civ. Eng.* **2023**, 1–17. [CrossRef]
30. Aggarwal, Y.; Saha, S.K. Seismic Performance Assessment of Reinforced Concrete Hilly Buildings with Open Story. *Structures* **2021**, *34*, 224–238. [CrossRef]

31. Balun, B. The Influence of Ground Motion Duration on the Energy Based Assessment of Buildings with Infill Walls. *Structures* **2023**, *49*, 765–778. [[CrossRef](#)]
32. IS-456:2000; Plain and Reinforced Concrete-Code of Practice Bureau of Indian Standards. Bureau of Indian Standards: New Delhi, India, 2000.
33. *Seismic Rehabilitation of Existing Buildings*; American Society of Civil Engineers: Reston, VA, USA, 2007. [[CrossRef](#)]
34. IS-1077:1992; Common Burnt Clay Building Bricks Specifications, BIS. Bureau of Indian Standards: New Delhi, India, 1992.
35. Mander, J.B.; Michael, J.N.P.; Park, R. Theoretical stress-strain model for confined concrete. *J. Struct. Eng.* **1988**, *114*, 1804–1826. [[CrossRef](#)]
36. FEMA-356; American Society of Civil Engineers. *Seismic Evaluation of Existing Buildings*; American Society of Civil Engineers: Reston, VA, USA, 2003. [[CrossRef](#)]
37. Choudhury, T.; Kaushik, H.B. Seismic Fragility of Open Ground Storey RC Frames with Wall Openings for Vulnerability Assessment. *Eng. Struct.* **2018**, *155*, 345–357. [[CrossRef](#)]
38. *Seismic Evaluation and Retrofit of Concrete Buildings (ATC-40)*; ATC (Applied Technology Council): Redwood, CA, USA, 1996.
39. Ghosh, B.; Pappin, J.; Arup, M.; Kong, H.; Arup, K. Dubai. Seismic Hazard Assessment in India. Available online: https://www.iitk.ac.in/nicee/wcee/article/WCEE2012_2107.pdf (accessed on 1 January 2017).
40. Morales-González, M.; Vidot-Vega, A.L. Seismic Response of Reinforced Concrete Frames at Different Damage Levels. *Int. J. Adv. Struct. Eng.* **2017**, *9*, 63–77. [[CrossRef](#)]
41. Skolnik, D.A.; Wallace, J.W. Critical Assessment of Interstory Drift Measurements. *J. Struct. Eng.* **2010**, *136*, 1574–1584. [[CrossRef](#)]

Disclaimer/Publisher’s Note: The statements, opinions and data contained in all publications are solely those of the individual author(s) and contributor(s) and not of MDPI and/or the editor(s). MDPI and/or the editor(s) disclaim responsibility for any injury to people or property resulting from any ideas, methods, instructions or products referred to in the content.